

Future snowfall in the Alps: Projections based on the EURO-CORDEX regional climate models

Prisco Frei¹, Sven Kotlarski^{2,*}, Mark A. Liniger², Christoph Schär¹

¹ Institute for Atmospheric and Climate Sciences, ETH Zurich, CH-8006 Zurich, Switzerland

² Federal Office of Meteorology and Climatology, MeteoSwiss, CH-8058 Zurich-Airport, Switzerland

* Corresponding author: sven.kotlarski@meteoswiss.ch

Abstract. Twenty-first century snowfall changes over the European Alps are assessed based on high-resolution regional climate model (RCM) data made available through the EURO-CORDEX initiative. Fourteen different combinations of global and regional climate models with a target resolution of 12 km, and two different emission scenarios are considered. As raw snowfall amounts are not provided by all RCMs, a newly developed method to separate snowfall from total precipitation based on near-surface temperature conditions and accounting for subgrid-scale topographic variability is employed. The evaluation of the simulated snowfall amounts against an observation-based reference indicates the ability of RCMs to capture the main characteristics of the snowfall seasonal cycle and its elevation dependency, but also reveals considerable positive biases especially at high elevations. These biases can partly be removed by the application of a dedicated RCM bias adjustment that separately considers temperature and precipitation biases.

Snowfall projections reveal a robust signal of decreasing snowfall amounts over most parts of the Alps for both emission scenarios. Domain and multi-model mean decreases of mean September-May snowfall by the end of the century amount to -25% and -45% for RCP4.5 and RCP8.5, respectively. Snowfall in low-lying areas in the Alpine forelands could be reduced by more than -80%. These decreases are driven by the projected warming and are strongly connected to an important decrease of snowfall frequency and snowfall fraction and are also apparent for heavy snowfall events. In contrast, high-elevation regions could experience slight snowfall increases in mid-winter for both emission scenarios despite the general decrease of the snowfall fraction. These increases in mean and heavy snowfall can be explained by a general increase of winter precipitation and by the fact that, with increasing temperatures, climatologically cold areas are shifted into a temperature interval which favours higher snowfall intensities. In general, percentage changes of snowfall indices are robust with respect to the RCM postprocessing strategy employed: Similar results are obtained for raw, separated and separated + bias-adjusted snowfall amounts. Absolute changes, however, can differ among these three methods.

38 **1 Introduction**

39 Snow is an important resource for the Alpine regions, be it for tourism, hydropower generation, or
40 water management (Abegg et al., 2007). According to the Swiss Federal Office of Energy (SFOE)
41 hydropower generation accounts for approximately 55% of the Swiss electricity production (SFOE,
42 2014). Consideration of changes in snow climatology needs to address aspects of both snow cover
43 and snowfall. In the recent past, an important decrease of the mean snow cover depth and duration in
44 the Alps was observed (e.g., Laternser and Schneebeli, 2003; Marty, 2008; Scherrer et al., 2004).
45 Projections of future snow cover changes based on climate model simulations indicate a further
46 substantial reduction (Schmucki et al., 2015a; Steger et al., 2013), strongly linked to the expected rise
47 of temperatures (e.g., CH2011, 2011; Gobiet et al., 2014). On regional and local scales rising
48 temperatures exert a direct influence on snow cover in two ways: First, total snowfall sums are
49 expected to decrease by a lower probability for precipitation to fall as snow implying a decreasing
50 snowfall fraction (ratio between solid and total precipitation). Second, snow on the ground is subject to
51 faster and accelerated melt. These warming-induced trends might be modulated by changes in
52 atmospheric circulation patterns.

53 Although the snowfall fraction is expected to decrease during the 21st century (e.g., Räisänen, 2016)
54 extraordinary snowfall events can still leave a trail of destruction. A recent example was the winter
55 2013/2014 with record-breaking heavy snowfall events along the southern rim of the European Alps
56 (e.g., Techel et al., 2015). The catastrophic effects of heavy snowfall range from avalanches and
57 floods to road or rail damage. In extreme cases these events can even result in the weight-driven
58 collapse of buildings or loss of human life (Marty and Blanchet, 2011). Also mean snowfall conditions,
59 such as the mean number of snowfall days in a given period, can be of high relevance for road
60 management (e.g. Zubler et al., 2015) or airport operation. Projections of future changes in snowfall,
61 including mean and extreme conditions, are therefore highly relevant for long-term planning and
62 adaptation purposes in order to assess and prevent related socio-economic impacts and costs.

63 21st century climate projections typically rely on climate models. For large-scale projections, global
64 climate models (GCMs) with a rather coarse spatial resolution of 100 km or more are used. To assess
65 regional to local scale impacts, where typically a much higher spatial resolution is required, a GCM
66 can be dynamically downscaled by nesting a regional climate model (RCM) over the specific domain
67 of interest (Giorgi, 1990). In such a setup, the GCM provides the lateral and sea surface boundary
68 conditions to the RCM. One advantage of climate models is the ability to estimate climate change in a
69 physically based manner under different greenhouse gas (GHG) emission scenarios. With the
70 Intergovernmental Panel on Climate Change's (IPCC) release of the Fifth Assessment Report (AR5;
71 IPCC, 2013) the so-called representative concentration pathway (RCP) scenarios have been
72 introduced (Moss et al., 2010) which specify GHG concentrations and corresponding emission
73 pathways for several radiative forcing targets. To estimate inherent projection uncertainties, ensemble
74 approaches employing different climate models, different greenhouse gas scenarios, and/or different
75 initial conditions are being used (e.g., Deser et al., 2012; Hawkins and Sutton, 2009; Rummukainen,
76 2010).

77 Within the last few years several studies targeting the future global and European snowfall evolution
78 based on climate model ensembles were carried out (e.g., de Vries et al., 2013; de Vries et al., 2014;
79 Krasting et al., 2013; O’Gorman, 2014; Piazza et al., 2014; Räisänen, 2016; Soncini and Bocchiola,
80 2011). Most of these analyses are based on GCM output or older generations of RCM ensembles at
81 comparatively low spatial resolution, which are not able to properly resolve snowfall events over
82 regions with complex topography. New generations of high resolution RCMs are a first step toward an
83 improvement on this issue. This is in particular true for the most recent high-resolution regional climate
84 change scenarios produced by the global CORDEX initiative (Giorgi et al., 2009) and its European
85 branch EURO-CORDEX (Jacob et al., 2014). The present work aims to exploit this recently
86 established RCM archive with respect to future snowfall conditions over the area of the European
87 Alps. It thereby complements the existing works of Piazza et al. (2014) and de Vries et al. (2014) who
88 among others also exploit comparatively high-resolved RCM experiments (partly originating from
89 EURO-CORDEX as well) but with a reduced ensemble size and/or not specifically targeting the entire
90 Alpine region.

91 In general and on decadal to centennial time scales, two main drivers of future snowfall changes over
92 the European Alps with competing effects on snowfall amounts are apparent from the available
93 literature: (1) Mean winter precipitation is expected to increase over most parts of the European Alps
94 and in most EURO-CORDEX experiments (e.g., Rajczak et al., in prep.; Smiatek et al., 2016) which in
95 principle could lead to higher snowfall amounts. (2) Temperatures are projected to considerably rise
96 throughout the annual cycle (e.g., Gobiet et al., 2014; Smiatek et al., 2016; Steger et al., 2013) with
97 the general effect of a decreasing snowfall frequency and fraction, thus potentially leading to a
98 reduction in overall snowfall amounts. Separating the above two competing factors is one of the
99 targets of the current study. A potential complication is that changes in daily precipitation frequency
100 (here events with precipitation > 1 mm/day) and precipitation intensity (average amount on wet days)
101 can change in a counteracting manner (e.g., Fischer et al., 2015; Rajczak et al., 2013), and that
102 relative changes are not uniform across the event category (e.g. Ban et al., 2015; Fischer and Knutti,
103 2016).

104 We here try to shed more light on these issues by addressing the following main objectives:

105 **Snowfall separation on an RCM grid.** Raw snowfall outputs are not available for all members of the
106 EURO-CORDEX RCM ensemble. Therefore, an adequate snowfall separation technique, i.e., the
107 derivation of snowfall amounts based on readily available daily near-surface air temperature and
108 precipitation data, is required. Furthermore, we seek for a snowfall separation method that accounts
109 for the topographic subgrid-scale variability of snowfall on the RCM grid.

110 **Snowfall bias adjustment.** Even the latest generation of RCMs is known to suffer from systematic
111 model biases (e.g., Kotlarski et al., 2014). In GCM-driven setups as employed within the present work
112 these might partly be inherited from the driving GCM. To remove such systematic model biases in
113 temperature and precipitation, a simple bias adjustment method is developed and employed in the
114 present work. To assess its performance and applicability, different snowfall indices in the bias-
115 adjusted and not bias-adjusted output are compared against observation-based estimates.

116 **Snowfall projections for the late 21st century.** Climate change signals for various snowfall indices
117 over the Alpine domain and for specific elevation intervals, derived by a comparison of 30-year control
118 and scenario periods, are analysed under the assumption of the RCP8.5 emission scenario. In
119 addition, we aim to identify and quantify the main drivers of future snowfall changes and, in order to
120 assess emission scenario uncertainties, compare RCP8.5-based results with experiments assuming
121 the more moderate RCP4.5 emission scenario. Snowfall projections are generally based on three
122 different datasets: (1) raw RCM snowfall where available, (2) RCM snowfall separated from simulated
123 temperature and precipitation, and (3) RCM snowfall separated from simulated temperature and
124 precipitation and additionally bias-adjusted. While all three estimates are compared for the basic
125 snowfall indices in order to assess the robustness of the projections, more detailed analyses are
126 based on dataset (3) only.

127 In addition and as preparatory analysis, we carry out a basic evaluation of RCM-simulated snowfall
128 amounts. This evaluation, however, is subject to considerable uncertainties as a high-quality
129 observation-based reference at the required spatial scale is not available, and the very focus of the
130 present work is laid on the snowfall projection aspect.

131 The article is structured as follows: Section 2 describes the data used and methods employed. In
132 Sections 3 and 4 results of the bias adjustment approach and snowfall projections for the late 21st
133 century are shown, respectively. The latter are further discussed in Section 5 while overall conclusions
134 and a brief outlook are provided in Section 6. Additional supporting figures are provided in the
135 supplementary material (prefix 'S' in Figure numbers).

136 **2 Data and methods**

137 **2.1 Observational data**

138 To estimate observation-based snowfall, two gridded data sets, one for precipitation and one for
139 temperature, derived from station observations and covering the area of Switzerland are used. Both
140 data sets are available on a daily basis with a horizontal resolution of 2 km for the entire evaluation
141 period 1971-2005 (see Sec. 2.3).

142 The gridded precipitation data set (RhiresD) represents a daily analysis based on a high-resolution
143 rain-gauge network (MeteoSwiss, 2013a) consisting of more than 400 stations that have a balanced
144 distribution in the horizontal but under-represent high altitudes (Frei and Schär, 1998; Isotta et al.,
145 2014; Konzelmann et al., 2007). Albeit the data set's resolution of 2 km, the effective grid resolution as
146 represented by the mean inter-station distance is about 15 - 20 km and thus comparable to the
147 nominal resolution of the available climate model data (see Sec. 2.2). The dataset has not been
148 corrected for the systematic measurement bias of rain gauges (e.g., Neff, 1977; Sevruk, 1985; Yang et
149 al., 1999).

150 The gridded near-surface air temperature (from now on simply referred to as *temperature*) data set
151 (TabsD) utilises a set of approx. 90 homogeneous long-term station series (MeteoSwiss, 2013b).
152 Despite the high quality of the underlying station series, errors might be introduced by unresolved

153 scales, an uneven spatial distribution and interpolation uncertainty (Frei, 2014). The unresolved effects
154 of land cover or local topography, for instance, probably lead to an underestimation of spatial
155 variability. Also note that, while RhiresD provides daily precipitation sums aggregated from 6 UTC to 6
156 UTC of the following day, TabsD is a true daily temperature average from midnight UTC to midnight
157 UTC. Due to a high temporal autocorrelation of daily mean temperature this slight inconsistency in the
158 reference interval of the daily temperature and precipitation grids is expected to not systematically
159 influence our analysis.

160 In addition to the gridded temperature and precipitation datasets and in order to validate simulated raw
161 snowfall amounts station-based observations of fresh snow sums (snow depth) at daily resolution from
162 29 stations in Switzerland with data available for at least 80% of the evaluation period 1971-2005 are
163 employed.

164 **2.2 Climate model data**

165 In terms of climate model data we exploit a recent ensemble of regional climate projections made
166 available by EURO-CORDEX (www.euro-cordex.net), the European branch of the World Climate
167 Research Programme's CORDEX initiative (www.cordex.org; Giorgi et al., 2009). RCM simulations for
168 the European domain were run at a resolution of approximately 50 km (EUR-44) and 12 km (EUR-11)
169 with both re-analysis boundary forcing (Kotlarski et al., 2014; Vautard et al., 2013) and GCM-forcing
170 (Jacob et al., 2014). We here disregard the reanalysis-driven experiments and employ the GCM-driven
171 simulations only. These include historical control simulations and future projections based on RCP
172 greenhouse gas and aerosol emission scenarios. Within the present work we employ daily averaged
173 model output of all except two ¹GCM-driven EUR-11 simulations for which control, RCP4.5 and
174 RCP8.5 runs were available in December 2016. This yields a total set of 14 GCM-RCM model chains,
175 combining five driving GCMs with seven different RCMs (Tab. 1). We exclusively focus on the higher
176 resolved EUR-11 simulations and disregard the coarser EUR-44 ensemble due to the apparent added
177 value of the EUR-11 ensemble with respect to regional-scale climate features in the complex
178 topographic setting of the European Alps (e.g., Giorgi et al., 2016; Torma et al., 2015).

179 It is important to note that each of the seven RCMs considered uses an individual grid cell topography
180 field. Model topographies for a given grid cell might therefore considerably differ from each other, and
181 also from the observation-based orography. Hence, it is not meaningful to compare snowfall values at
182 individual grid cells since the latter might be situated at different elevations. Therefore, most analyses
183 of the present work were carried out as a function of elevation, i.e., by averaging climatic features over
184 distinct elevation intervals.

185 **2.3 Analysis domain and periods**

186 The arc-shaped European Alps - with a West-East extent of roughly 1200 km , a total of area 190'000
187 km² and a peak elevation of 4810 m a.s.l. (Mont Blanc) - are the highest and most prominent

¹ The HadGEM2-RACMO experiments were excluded due to serious snow accumulation issues over the European Alps. Furthermore, only realization 1 of MPI-M-REMO was included in order to avoid mixing GCM-RCM sampling with pure internal climate variability sampling.

188 mountain range which is entirely situated in Europe. In the present work, two different analysis
189 domains are used. The evaluation of the bias adjustment approach depends on the observational data
190 sets RhiresD and TabsD (see Sec. 2.1). As these cover Switzerland only, the evaluation part of the
191 study (Sec. 3) is constrained to the Swiss domain (Fig. 1, bold line). For the analysis of projected
192 changes of different snowfall indices (Sec. 4 and 5) a larger domain covering the entire Alpine crest
193 with its forelands is considered (Fig. 1, coloured region).

194 Our analysis is based on three different time intervals. The evaluation period (EVAL) 1971-2005 is
195 used for the calibration and validation of the bias adjustment approach. Future changes of snowfall
196 indices are computed by comparing a present-day control period (1981-2010, CTRL) to a future
197 scenario period at the end of the 21st century (2070-2099, SCEN). For all periods (EVAL, CTRL and
198 SCEN), the summer months June, July and August (JJA) are excluded from any statistical analysis. In
199 addition to seasonal mean snowfall conditions, i.e., averages over the nine-month period from
200 September to May, we also analyse the seasonal cycle of individual snowfall indices at monthly
201 resolution.

202 **2.4 Analysed snowfall indices and change signals**

203 A set of six different snowfall indices is considered (Tab. 2). Mean snowfall (S_{mean}) refers to the
204 (spatio-) temporally-averaged snowfall amount in mm SWE (note that from this point on we will use the
205 term "mm" as a synonym for "mm SWE" as unit of several snowfall indices). The two indices heavy
206 snowfall (S_{q99}) and maximum 1-day snowfall (S_{1d}) allow the assessment of projected changes in heavy
207 snowfall events and amounts. S_{1d} is derived by averaging maximum 1-day snowfall amounts over all
208 individual months/seasons of a given time period (i.e., by averaging 30 maximum values in the case of
209 the CTRL and SCEN period), while S_{q99} is calculated from the grid point-based 99th all-day snowfall
210 percentile of the daily probability density function (PDF) for the entire time period considered. We use
211 all-day percentiles as the use of wet-day percentiles leads to conditional statements that are often
212 misleading (see the analysis in Schär et al. 2016). Note that the underlying number of days differs for
213 seasonal (September-May) and monthly analyses. Snowfall frequency (S_{freq}) and mean snowfall
214 intensity (S_{int}) are based on a wet-day threshold of 1 mm/day and provide additional information about
215 the distribution and magnitude of snowfall events, while the snowfall fraction (S_{frac}) describes the ratio
216 of solid precipitation to total precipitation. As climate models tend to suffer from too high occurrence of
217 drizzle and as small precipitation amounts are difficult to measure, daily precipitation values smaller or
218 equal to 0.1 mm were set to zero in both the observations and the simulations prior to the remaining
219 analyses.

220 Projections are assessed by calculating two different types of changes between the CTRL and the
221 SCEN period. The absolute change signal (Δ) of a particular snowfall index X (see Tab.2)

$$222 \Delta X = X_{SCEN} - X_{CTRL} \quad (1)$$

223 and the relative change signal (δ) which describes the change of the snowfall index as a percentage of
224 its CTRL period value

$$225 \quad \delta X = \left(\frac{X_{SCEN}}{X_{CTRL}} - 1 \right) \cdot 100 \quad (2)$$

226 To prevent erroneous data interpretation due to possibly large relative changes of small CTRL values,
 227 certain grid boxes were masked out before calculating and averaging the signal of change. This
 228 filtering was done by setting threshold values for individual indices and statistics (see Table 2).

229 **2.5 Separating snowfall from total precipitation**

230 Due to (a) the lack of a gridded observational snowfall data set and (b) the fact that not all RCM
 231 simulations available through EURO-CORDEX provide raw snowfall as an output variable, a method
 232 to separate solid from total precipitation depending on near-surface temperature conditions is
 233 developed. The simplest approach to separate snowfall from total precipitation is to fractionate the two
 234 phases binary by applying a constant snow fractionation temperature (e.g., de Vries et al., 2014;
 235 Schmucki et al., 2015a; Zubler et al., 2014). More sophisticated methods estimate the snow fraction f_s
 236 dependence on air temperature with linear or logistic relations (e.g., Kienzle, 2008; McAfee et al.,
 237 2014). In our case, the different horizontal resolutions of the observational (high resolution of 2 km)
 238 and simulated (coarser resolution of 12 km) data sets further complicate a proper comparison of the
 239 respective snowfall amounts. Thus, we explicitly analysed the snowfall amount dependency on the
 240 grid resolution and exploited possibilities for including subgrid-scale variability in snowfall separation.
 241 This approach is important as especially in Alpine terrain a strong subgrid-scale variability of near-
 242 surface temperatures due to orographic variability has to be expected, with corresponding effects on
 243 the subgrid-scale snowfall fraction.

244 For this preparatory analysis, which is entirely based on observational data, a reference snowfall is
 245 derived. It is based on the approximation of snowfall by application of a fixed temperature threshold to
 246 daily total precipitation amounts on the high resolution observational grid (2 km) and will be termed
 247 *Subgrid method* thereafter: First, the daily snowfall S' at each grid point of the observational data set at
 248 high resolution (2 km) is derived by applying a snow fractionation temperature $T^*=2^\circ\text{C}$. The whole
 249 daily precipitation amount P' is accounted for as snow S' (i.e., $f_s=100\%$) for days with daily mean
 250 temperature $T \leq T^*$. For days with $T > T^*$, S' is set to zero and P' is attributed as rain (i.e., $f_s=0\%$). This
 251 threshold approach with a fractionation temperature of 2°C corresponds to the one applied in previous
 252 works and results appear to be in good agreement with station-based snowfall measurements (e.g.,
 253 Zubler et al., 2014). The coarse grid (12 km) reference snowfall S_{SG} is determined by averaging the
 254 sum of separated daily high resolution S' over all n high-resolution grid points i located within a specific
 255 coarse grid point k . I.e., at each coarse grid point k

$$256 \quad S_{SG} = \frac{1}{n} \cdot \sum_{i=1}^n P'_i [T'_i \leq T^*] = \frac{1}{n} \sum_{i=1}^n S'_i \quad (3)$$

257 For comparison, the same binary fractionation method with a temperature threshold of $T^*=2^\circ\text{C}$ is
 258 directly applied on the coarse 12 km grid (*Binary method*). For this purpose, total precipitation P' and
 259 daily mean temperature T' of the high-resolution data are conservatively remapped to the coarse grid
 260 leading to P and T , respectively. Compared to the *Subgrid method*, the *Binary method* neglects any
 261 subgrid-scale variability of the snowfall fraction. As a result, the *Binary method* underestimates S_{mean}

262 and overestimates S_{q99} for most elevation intervals (Fig. 2). The underestimation of S_{mean} can be
 263 explained by the fact that even for a coarse grid temperature above T^* individual high-elevation
 264 subgrid cells (at which $T \leq T^*$) can receive substantial snowfall amounts. As positive precipitation-
 265 elevation gradients can be assumed for most parts of the domain (larger total precipitation at high
 266 elevations; see e.g. Kotlarski et al., 2012 and Kotlarski et al., 2015 for an Alpine-scale assessment)
 267 the neglect of subgrid-scale snowfall variation in the *Binary method* hence leads a systematic
 268 underestimation of mean snowfall compared to the *Subgrid method*. Furthermore, following O’Gorman
 269 (2014), heavy snowfall events are expected to occur in a narrow temperature range below the rain-
 270 snow transition. As the *Binary method* in these temperature ranges always leads to a snowfall fraction
 271 of 100%, too large S_{q99} values would result.

272 To take into account these subgrid-scale effects, a more sophisticated approach – referred to as the
 273 *Richards method* – is developed here. This method is based upon a generalised logistic regression
 274 (Richards, 1959). Here, we apply this regression to relate the surface temperature T to the snow
 275 fraction f_s by accounting for the topographic subgrid-scale variability. At each coarse grid-point k , the
 276 *Richards method*-based snowfall fraction $f_{s,RI}$ for a given day is hence computed as follows:

$$277 \quad f_{s,RI}(T_k) = \frac{1}{[1 + C_k \cdot e^{D_k \cdot (T_k - T^*)}]^{1/C_k}} \quad (4)$$

278 with C as the point of inflexion (denoting the point with largest slope), and D the growth rate (reflecting
 279 the mean slope). T_k is the daily mean temperature of the corresponding coarse grid box k and $T^*=2^\circ\text{C}$
 280 the snow fractionation temperature. First, we estimate the two parameters C and D of Equation 4 for
 281 each single coarse grid point k by minimizing the least-square distance to the f_s values derived by the
 282 *Subgrid method* via the reference snowfall S_{SG} (local fit). Second, C and D are expressed as a function
 283 of the topographic standard deviation σ_h of the corresponding coarse resolution grid point only (Fig.
 284 S1; global fit). This makes it possible to define empirical functions for both C and D that can be used
 285 for all grid points k in the Alpine domain and that depend on σ_h only.

$$286 \quad \sigma_{h,k} = \sqrt{\frac{\sum_{i=1}^n (h_i - \bar{h}_k)^2}{n-1}} \quad (5)$$

$$287 \quad C_k = \frac{1}{(E - \sigma_{h,k} \cdot F)} \quad (6)$$

$$288 \quad D_k = G \cdot \sigma_{h,k}^{-H} \quad (7)$$

289 Through a minimisation of the least square differences the constant parameters in Equations 6 and 7
 290 are calibrated over the domain of Switzerland and using daily data from the period September to May
 291 1971-2005 leading to values of $E=1.148336$, $F=0.000966 \text{ m}^{-1}$, $G=143.84113 \text{ }^\circ\text{C}^{-1}$ and $H=0.8769335$.
 292 Note that σ_h is sensitive to the resolution of the two grids to be compared (cf. Eq. 5). It is a measure for
 293 the uniformity of the underlying topography and has been computed based on the high-resolution
 294 GTOPO30 digital elevation model (<https://lta.cr.usgs.gov/GTOPO30>) aggregated to a regular grid of
 295 1.25 arc seconds (about 2 km) which reflects the spatial resolution of the observed temperature and
 296 precipitation grids (cf. Section 2.1). Small values of σ_h indicate a low subgrid-scale topographic

297 variability, such as in the Swiss low-lands, while high values result from non-uniform elevation
298 distributions, such as in areas of inner Alpine valleys. σ_h as derived from GTOPO30 might be different
299 from the subgrid-scale topographic variance employed by the climate models themselves, which is
300 however not relevant here as only grid cell-averaged model output is analysed and as we consider σ_h
301 as a proper estimate of subgrid-scale variability.

302 Figure S1 (panel c) provides an example of the relation between daily mean temperature and daily
303 snow fraction f_s for grid cells with topographical standard deviations of 50 m and 500 m, respectively.
304 The snowfall amount S_{RI} for a particular day and a particular coarse grid box is finally obtained by
305 multiplying the corresponding $f_{s,RI}$ and P values. A comparison with the *Subgrid method* yields very
306 similar results. For both indices S_{mean} and S_{q99} , mean ratios across all elevation intervals are close to 1
307 (Fig. 2). At single grid points, maximum deviations are not larger than 1 ± 0.1 . Note that for this
308 comparison calibration and validation period are identical (EVAL period). Based on this analysis, it has
309 been decided to separate snowfall according to the *Richards method* throughout this work in both the
310 observations and in the RCMs. The observation-based snowfall estimate obtained by applying the
311 *Richards method* to the observational temperature and precipitation grids after spatial aggregation to
312 the 0.11° RCM resolution will serve as reference for the RCM bias adjustment and will be termed
313 *reference* hereafter. One needs to bear in mind that the parameters C and D of the Richards method
314 were fitted for the Swiss domain only and were later on applied to the entire Alpine domain (cf. Fig. 1).

315 **2.6 Bias adjustment approach**

316 Previous work has revealed partly substantial temperature and precipitation biases of the EURO-
317 CORDEX RCMs over the Alps (e.g. Kotlarski et al., 2014; Smiatek et al., 2016), and one has to expect
318 that the separated snowfall amounts are biased too. This would especially hamper the interpretation of
319 absolute climate change signals of the considered snow indices. We therefore explore possibilities to
320 bias-adjust the simulated snowfall amounts and to directly integrate this bias adjustment into the
321 snowfall separation framework of Section 2.5. Note that we deliberately employ the term *bias*
322 *adjustment* as opposed to *bias correction* to make clear that only certain aspects of the snowfall
323 climate are adjusted and that the resulting dataset might be subject to remaining inaccuracies.

324 A simple two-step approach that separately accounts for precipitation and temperature biases and
325 their respective influence on snowfall is chosen. The separate consideration of temperature and
326 precipitation biases allows for a more physically-based bias adjustment of snowfall amounts: Due to
327 the temperature dependency of snowfall occurrence, snowfall biases of a given climate model cannot
328 be expected to remain constant under current and future (i.e., warmer) climate conditions. For
329 instance, a climate model with a given temperature bias might pass the snow-rain temperature
330 threshold earlier or later than reality during the general warming process. Hence, traditional bias
331 adjustment approaches based only on a comparison of observed and simulated snowfall amounts in
332 the historical climate would possibly fail due to a non-stationary bias structure. The bias adjustment is
333 calibrated in the EVAL period for each individual GCM-RCM chain and over the region of Switzerland,
334 and is then applied to both the CTRL and SCEN period of each chain and for the entire Alpine domain.

335 To be consistent in terms of horizontal grid spacing, the observational data sets RhiresD and TabsD
336 (see Sec. 2.1) are conservatively regridded to the RCM resolution beforehand.

337 In a first step, total simulated precipitation was adjusted by introducing an elevation-dependent
338 adjustment factor which adjusts precipitation biases regardless of temperature. For this purpose, mean
339 precipitation ratios (RCM simulation divided by observational analysis) for 250 m elevation intervals
340 were calculated (Fig. S2). An almost linear relationship of these ratios with elevation was found. Thus,
341 a linear regression between the intervals from 250 m a.s.l. to 2750 m a.s.l. was used for each model
342 chain separately to estimate a robust adjustment factor. As the number of both RCM grid points and
343 measurement stations at very high elevations (>2750 m a.s.l.) is small (see Sec. 2.1) and biases are
344 subject to a considerable sampling uncertainty, these elevations were not considered in the
345 regression. Overall the fits are surprisingly precise except for the altitude bins above 2000 m (Fig. S2).
346 The precipitation adjustment factors (P_{AF}) for a given elevation were then obtained as the inverse of
347 the fitted precipitation ratios. Multiplying simulated precipitation P with P_{AF} for the respective model
348 chain and elevation results in the adjusted precipitation:

$$349 \quad P_{adj} = P \cdot P_{AF} \quad (8)$$

350 For a given GCM-RCM chain and for each elevation interval, the spatially and temporally averaged
351 corrected total precipitation P_{adj} approximately corresponds to the observation-based estimate in the
352 EVAL period.

353 In the second step of the bias adjustment procedure, temperature biases are accounted for. For this
354 purpose the initial snow fractionation temperature $T^*=2^\circ\text{C}$ of the Richards separation method (see Sec
355 2.5) is shifted to the value T_a^* for which the spatially (Swiss domain) and temporally (September to
356 May) averaged simulated snowfall amounts for elevations below 2750 m a.s.l. match the respective
357 observation-based reference (see above). Compared to the adjustment of total precipitation, T_a^* is
358 chosen independent of elevation but separately for each GCM-RCM chain, in order to avoid
359 overparameterization and to not over-interpret the elevation dependency of mean snowfall in the
360 snowfall reference grid. After this second step of the bias adjustment, the spatially and temporally
361 averaged simulated snowfall amounts below 2750 m a.s.l. match the reference by definition. Hence,
362 the employed simple bias adjustment procedure adjusts domain-mean snowfall biases averaged over
363 the entire season from September to May. It does, however, not correct for biases in the spatial
364 snowfall pattern, in the seasonal cycle, or in the temporal distribution of daily values. Note that, as the
365 underlying high-resolution data sets are available over Switzerland only, the calibration of the bias
366 adjustment methodology is correspondingly restricted, but the adjustment is then applied to the whole
367 Alpine domain. This approach is justified as elevation-dependent mean winter precipitation and
368 temperature biases of the RCMs employed – assessed by comparison against the coarser-resolved
369 EOBS reference dataset (Haylock et al., 2008) - are very similar for Switzerland and for the entire
370 Alpine analysis domain (Figs. S3 and S4).

371 **3 Evaluation**

372 **3.1 RCM raw snowfall**

373 We first carry out an illustrative comparison of RCM raw snowfall amounts (for those simulations only
374 that directly provide snowfall flux) against station observations of snowfall in order to determine
375 whether the simulated RCM snowfall climate contains valid information despite systematic biases. To
376 this end, simulated raw snowfall amounts of nine EURO-CORDEX simulations (see Tab. 1) averaged
377 over 250 m-elevation intervals and over the range 950 – 1650 m a.s.l. are compared against
378 observations of measured fresh snow sums from 29 MeteoSwiss stations (see Section 2.1).. For this
379 purpose a mean snow density of 100 kg/m^3 for the conversion from measured snow depth to water
380 equivalent is assumed. Note that this simple validation is subject to considerable uncertainties as it
381 does not explicitly correct for the scale and elevation gap between grid-cell based RCM output and
382 single-site observations. Especially in complex terrain and for exposed sites, point measurements of
383 snow depth might be non-representative for larger-scale conditions (e.g., Grünewald and Lehning,
384 2015). Also, the conversion from snow depth to snow water equivalent is of approximate nature only,
385 and fresh snow sums might furthermore misrepresent true snowfall in case that snow melt or snow
386 drift occurs between two snow depth readings.

387 At low elevations simulated mean September-May raw snowfall sums match the observations well
388 while differences are larger aloft (Fig. 3a). The positive bias at high elevations might arise from the fact
389 that (the very few) observations were made at specific locations while simulated grid point values of
390 the corresponding elevation interval might be located in different areas of Switzerland. It might also be
391 explained by positive RCM precipitation and negative RCM temperature biases at high elevations of
392 the Alps (e.g., Kotlarski et al., 2015). At lower elevations, the station network is geographically more
393 balanced and the observations are probably more representative of the respective elevation interval.
394 Despite a clear positive snowfall bias in mid-winter, the RCMs are generally able to reproduce the
395 mean seasonal cycle of snowfall for elevations between 950 m a.s.l. - 1650 m a.s.l. (Fig. 3b). The fact
396 that the major patterns of both the snowfall-elevation relationship and the mean seasonal snowfall
397 cycle are well represented indicates the general and physically consistent applicability of RCM output
398 to assess future changes in mean and heavy Alpine snowfall. However, substantial biases in snowfall
399 amounts are apparent and a bias adjustment of simulated snowfall seems to be required prior to the
400 analysis of climate change signals of individual snowfall indices.

401 **3.2 Evaluation of the reference snowfall**

402 The snowfall separation employing the *Richards method* (Section 2.5) and, as a consequence, also
403 the bias adjustment (Section 2.6) make use of the 2 km reference snowfall grid derived by employing
404 the *Subgrid method* on the observed temperature and precipitation grids. Hence, the final results of
405 this study could to some extent be influenced by inaccuracies and uncertainties of the reference
406 snowfall grid itself. In order to assess the quality of the latter and in absence of a further observation-
407 based reference we here present an approximate evaluation.

408 First, the reference snowfall grid is evaluated against fresh snow sums at the 29 Swiss stations that
409 were also used for evaluating RCM raw snowfall. Note the limitations of such a comparison as outlined
410 in Chapter 3.1. The comparison of black and red markers and lines in Figure 3 indicates a good
411 agreement of mean snowfall at individual elevation intervals (left panel) as well for the mean annual
412 cycle of snowfall at medium elevations (right panel). The reference snowfall grid is obviously a good
413 approximation of site-scale fresh snow sums. Note that similarly to the RCM raw snowfall evaluation,
414 all 2 km reference snowfall grid cells in the respective elevation interval are considered. The good
415 agreement, however, still holds if only those 2 km grid cells covering the 29 site locations are
416 considered (not shown here).

417 Second, both the 2 km reference snowfall grid and the 0.11° reference snowfall grid obtained by
418 employing the Richards method to aggregated temperature and precipitation values (see Section 2.5)
419 are compared against the gridded HISTALP dataset of solid precipitation (Chimani et al., 2011). The
420 latter is provided at a monthly resolution on a 5' grid covering the Greater Alpine Region. It is based on
421 monthly snowfall fraction estimates that are used to scale a gridded dataset of total precipitation. The
422 comparison of the three datasets for the region of Switzerland (for which the 2 km reference snowfall
423 is available) in the EVAL period 1971-2005 yields an approximate agreement of both the magnitude of
424 mean winter snowfall and its spatial pattern. The three data sets differ with respect to their spatial
425 resolution but all show a clear dependency of snowfall on topography and mean September-May
426 snowfall sums above 1000 mm over most parts of the Alpine ridge. Climatologically warm and dry
427 valleys, on the other hand, are represented by minor snowfall amounts of less than 400 mm only.

428 As mentioned before these evaluations of the reference snowfall grid are subject to uncertainties and,
429 furthermore, they only cover mean snowfall amounts. However, they provide basic confidence in the
430 applicability of the reference snowfall grid for the purposes of snowfall separation and bias adjustment
431 in the frame of the present study.

432

433 **3.3 Calibration of bias adjustment**

434 The analysis of total precipitation ratios (RCM simulations with respect to observations) for the EVAL
435 period, which are computed to carry out the first step of the bias adjustment procedure, reveals
436 substantial elevation dependencies. All simulations tend to overestimate total precipitation at high
437 elevations (Fig. S2). This fact might ultimately be connected to an overestimation of surface snow
438 amount in several EURO-CORDEX RCMs as reported by Terzago et al. (2017). As the precipitation
439 ratio between simulations and observations depends approximately linearly on elevation, the
440 calculation of P_{AF} via a linear regression of the ratios against elevation (see Sec. 2.6) seems
441 reasonable. By taking the inverse of this linear relation, P_{AF} for every model and elevation can be
442 derived. For the CCLM and RACMO simulations, these correction factors do not vary much with
443 height, while P_{AF} for MPI-ESM - REMO and EC-EARTH - HIRHAM is much larger than 1 in low lying
444 areas, indicating a substantial underestimation of observed precipitation sums (Fig. 4a). However, for
445 most elevations and simulations, P_{AF} is generally smaller than 1, i.e., total precipitation is
446 overestimated by the models. Similar model biases in the winter and spring seasons have already

447 been reported in previous works (e.g., Rajczak et al., in prep.; Smiatek et al., 2016). Especially at high
448 elevations, these apparent positive precipitation biases could be related to observational undercatch,
449 i.e., an underestimation of true precipitation sums by the observational analysis. Frei et al. (2003)
450 estimated seasonal Alpine precipitation undercatch for three elevation intervals. Results show that
451 measurement biases are largest in winter and increase with altitude. However, a potential undercatch
452 (with a maximum of around 40% at high elevations in winter; Frei et al., 2003) can only partly explain
453 the partly substantial overestimation of precipitation found in the present work.

454 After applying P_{AF} to the daily precipitation fields, a snowfall fractionation at the initial T^* of 2 °C (see
455 Eq. (4)) would lead to a snowfall excess in all 14 simulations as models typically experience a cold
456 winter temperature bias. To match the observation-based and spatio-temporally averaged reference
457 snowfall below 2750 m a.s.l., T^* for all models needs to be decreased during the second step of the
458 bias adjustment (Fig 4b). The adjusted T_a^* values indicate a clear positive relation with the mean
459 temperature bias in the EVAL period. This feature is expected since the stronger a particular model's
460 cold bias the stronger the required adjustment of the snow fractionation temperature T^* towards lower
461 values in order to avoid a positive snowfall bias. Various reasons for the scatter around a simple linear
462 relation in Figure 4b can be thought of. These include remaining spatial inaccuracies of the corrected
463 precipitation grid, elevation-dependent temperature biases and misrepresented temperature-
464 precipitation relationships at daily scale. Note that precipitation and temperature biases heavily
465 depend on the GCM-RCM chain and seem to be rather independent from each other. While EC-
466 EARTH – RACMO, for instance, shows one of the best performances in terms of total precipitation, its
467 temperature bias close to -5 °C is the largest deviation in our set of simulations. Concerning the partly
468 substantial temperature biases of the EURO-CORDEX models shown in Figure 4 b, their magnitude
469 largely agrees with Kotlarski et al. (2014; in reanalysis-driven simulations) and Smiatek et al. (2016).

470 **3.4 Evaluation of snowfall indices**

471 We next assess the performance of the bias adjustment procedure by comparing snowfall indices
472 derived from separated and bias-adjusted RCM snowfall amounts against the observation-based
473 reference. The period for which this comparison is carried out is EVAL, i.e., it is identical to the
474 calibration period of the bias adjustment. We hence do not intend a classical cross validation exercise
475 with separate calibration and validation periods, but try to answer the following two questions: (a)
476 Which aspects of the Alpine snowfall climate are adjusted, and (b) for which aspects do biases remain
477 even after application of the bias adjustment procedure.

478 Figure 5 shows the evaluation results of the six snowfall indices based on the separated and not bias-
479 adjusted simulated snowfall ($RCM_{sep+nba}$), and the separated and bias-adjusted simulated snowfall
480 (RCM_{sep+ba}). In the first case the snowfall separation of raw precipitation is performed with $T^*=2^\circ\text{C}$,
481 while in the second case precipitation is adjusted and the separation is performed with a bias-adjusted
482 temperature T_a^* . The first column represents the mean September to May statistics, while columns 2-4
483 depict the seasonal cycle at monthly resolution for three distinct elevation intervals.

484 The analysis of S_{mean} confirms that $\text{RCM}_{\text{sep+ba}}$ is able to reproduce the observation-based reference in
485 the domain mean as well as in most individual elevation intervals. The domain-mean agreement is a
486 direct consequence of the design of the bias adjustment procedure (see above). $\text{RCM}_{\text{sep+nba}}$, on the
487 other hand, consistently overestimates S_{mean} by up to a factor of 2.5 as a consequence of positive
488 precipitation and negative temperature biases (cf. Fig. 4). Also the seasonal cycle of S_{mean} for
489 $\text{RCM}_{\text{sep+ba}}$ yields a satisfying performance across all three elevation intervals, while $\text{RCM}_{\text{sep+nba}}$ tends
490 to produce too much snowfall over all months and reveals an increasing model spread with elevation.

491 For the full domain and elevations around 1000 m, the observation-based reference indicates a mean
492 S_{freq} of 20% between September and May. Up to 1000 m a.s.l. $\text{RCM}_{\text{sep+ba}}$ reflects the increase of this
493 index with elevation adequately. However, towards higher elevations the approximately constant S_{freq}
494 of 30% in the reference is not captured by the simulation-derived snowfall. Notably during wintertime,
495 both $\text{RCM}_{\text{sep+ba}}$ and $\text{RCM}_{\text{sep+nba}}$ produce too many snowfall days, i.e., overestimate snowfall
496 frequency. This feature is related to the fact that climate models typically tend to overestimate the wet
497 day frequency over the Alps especially in wintertime (Rajczak et al., 2013) and that the bias
498 adjustment procedure employed does not explicitly correct for potential biases in precipitation
499 frequency. Due to the link between mean snowfall on one side and snowfall frequency and mean
500 intensity on the other side, opposite results are obtained for the mean snowfall intensity S_{int} . $\text{RCM}_{\text{sep+ba}}$
501 largely underestimates mean intensities during snowfall days while $\text{RCM}_{\text{sep+nba}}$ typically better reflects
502 the reference. Nevertheless, deviations during winter months at mid-elevations are not negligible.
503 Mean September-May S_{frac} in the reference exponentially increases with elevation. This behaviour is
504 reproduced by both $\text{RCM}_{\text{sep+ba}}$ and $\text{RCM}_{\text{sep+nba}}$. Notwithstanding, $\text{RCM}_{\text{sep+ba}}$ results are more accurate
505 compared to $\text{RCM}_{\text{sep+nba}}$, which turns out to be biased towards too large snowfall fractions.

506 For the two heavy snowfall indices S_{q99} and S_{1d} , $\text{RCM}_{\text{sep+nba}}$ appears to typically match the reference
507 better than $\text{RCM}_{\text{sep+ba}}$. Especially at high elevations, $\text{RCM}_{\text{sep+ba}}$ produces too low snowfall amounts.
508 This again illustrates the fact that the bias adjustment procedure is designed to adjust biases in mean
509 snowfall, but does not necessarily improve further aspects of the simulated snowfall climate.

510 The spatial patterns of S_{mean} for the 14 $\text{RCM}_{\text{sep+ba}}$ simulations from September to May are presented in
511 Figure 6. The observational-based reference (lower right panel) reveals a snowfall distribution with
512 highest values along the Alpine main ridge, whereas the Swiss plateau, Southern Ticino and main
513 valleys such as the Rhône and Rhine valley experience less snowfall. Almost all bias-adjusted models
514 are able to represent the overall picture with snow-poor lowlands and snow-rich Alpine regions.
515 Nevertheless substantial differences to the observations concerning the spatial snowfall pattern can
516 arise. EC-EARTH - HIRHAM, for example, is subject to a "pixelated" structure. This could be the result
517 of frequent grid-cell storms connected to parameterisations struggling with complex topographies.
518 Such inaccuracies in the spatial pattern are not corrected for by our simple bias adjustment approach
519 which only targets domain-mean snowfall amounts at elevations below 2750 m a.s.l. and that does not
520 considerably modify the simulated spatial snowfall patterns.. Note that these patterns are obviously
521 strongly determined by the RCM itself and only slightly depend on the driving GCM (see, for instance,
522 the good agreement among the CCLM and the RCA simulations).

523 In summary, after applying the bias adjustment to the simulations most snowfall indices are fairly well
524 represented at elevations below 1000 m a.s.l.. With increasing altitude and smaller sample sizes in
525 terms of number of grid cells, reference and RCM_{sep+ba} diverge. This might be caused by the remaining
526 simulated overestimation of S_{freq} and an underestimation of S_{int} . While the bias adjustment approach
527 leads to a reduction of S_{int} due to the total precipitation adjustment, S_{freq} is only slightly modified by this
528 correction and by the adjustment of T^* . Nevertheless, these two parameters strongly influence other
529 snowfall indices. The counteracting effects of overestimated S_{freq} and underestimated S_{int} result in
530 appropriate amounts of S_{mean} whereas discrepancies for S_{q99} and S_{1d} are mainly driven by the
531 underestimation of S_{int} .

532 **4 Snowfall projections for the late 21st century**

533 For the study of climate change signals, the analysis domain is extended to the entire Alps (see Sec.
534 2.3). Due to the identified difficulties of bias-adjusting certain snowfall indices (see Sec 3.4), emphasis
535 is laid upon relative signals of change (see Eq. 2). This type of change can be expected to be less
536 dependent on the remaining inaccuracies after the adjustment. If not stated otherwise, all results in
537 this Section are based on the RCM_{sep+ba} data, i.e., on separated and bias-adjusted RCM snowfall, and
538 on the RCP8.5 emission scenario.

539 Projections for seasonal S_{mean} show a considerable decrease over the entire Alpine domain (Fig. 7).
540 Most RCMs project largest percentage losses of more than 80% across the Alpine forelands and
541 especially in its topographic depressions such as the Po and Rhone valleys. Over the Alpine ridge,
542 reductions are smaller but still mostly negative. Elevated regions between Southeastern Switzerland,
543 Northern Italy and Austria seem to be least affected by the overall snowfall reduction. Some of the
544 simulations (e.g., CNRM-RCA, MPI-ESM-RCA or MPI-ESM-REMO) project only minor changes in
545 these regions. Experiments employing the same RCM but different driving GCMs (e.g. the four
546 simulations of RCA), but also experiments employing the same GCM but different RCMs (e.g. the four
547 simulations driven by EC-EARTH, though different realizations) can significantly disagree in regional-
548 scale change patterns and especially in the general magnitude of change. This highlights a strong
549 influence of both the driving GCMs and the RCMs themselves on snowfall changes, representing
550 effects of large-scale circulation and meso-scale response, respectively.

551 A more detailed analysis is provided in Fig. 8 which addresses the vertical and seasonal distribution of
552 snowfall changes. It reveals that relative (seasonal mean) changes of S_{mean} appear to be strongly
553 dependent on elevation (Fig.8, top left panel). The multi-model mean change ranges from -80% at low
554 elevations to -10% above 3000 m a.s.l.. Largest differences between neighbouring elevation intervals
555 are obtained from 750 m a.s.l. to 1500 m a.s.l.. Over the entire Alps, the results show a reduction of
556 S_{mean} by -35% to -55% with a multi-model mean of -45%. The multi-model spread appears to be rather
557 independent of elevation and is comparably small, confirming that, overall, the spatial distributions of
558 the change patterns are similar across all model chains (cf. Fig. 7). All simulations point to decreases
559 over the entire nine-month period September to May for the two elevation intervals <1000 m a.s.l. and
560 1000 to 2000 m a.s.l.. Above 2000 m a.s.l., individual simulations show an increase of S_{mean} by up to

561 20% in mid-winter which leads to a slightly positive change in multi-model mean in January and
562 February.

563 Decreases of S_{freq} are very similar to changes in mean snowfall. Mean September-May changes are
564 largest below 1000 m a.s.l., while differences among elevation intervals become smaller at higher
565 elevations. In-between is a transition zone with rather strong changes with elevation, which
566 approximately corresponds to the mean elevation of the September-May zero-degree line in today's
567 climate (e.g., Ceppi et al., 2012; MeteoSchweiz, 2016). Individual simulations with large reductions in
568 S_{mean} , such as the RCA experiments, also project strongest declines in S_{freq} . In contrast, the mean
569 snowfall intensity S_{int} is subject to smallest percentage variations in our set of snowfall indices. Strong
570 percentage changes for some models in September are due to the small sample size (only few grid
571 points considered) and the low snowfall amounts in this month. Apart from mid elevations with
572 decreases of roughly -10%, mean intensities from September to May are projected to remain almost
573 unchanged by the end of the century. For both seasonal and monthly changes, model agreement is
574 best for high elevations while the multi-model spread is largest for lowlands. Large model spread at
575 low elevations might be caused by the small number of grid points used for averaging over the
576 respective elevation interval, especially in autumn and spring.

577 Similar results are obtained for the heavy snowfall indices S_{q99} and S_{1d} . While percentage decreases
578 at lowermost elevations are even larger than for S_{mean} , losses at high elevations are less pronounced,
579 resulting in similar domain-mean change signals for heavy and mean snowfall. Substantial differences
580 between monthly δS_{q99} and δS_{1d} appear at elevations below 1000 m a.s.l.. Here, percentage losses of
581 S_{q99} are typically slightly more pronounced. Above 2000 m a.s.l. both indices appear to remain almost
582 constant between January and March with change signals close to zero. The multi-model mean
583 changes even hint to slight increases of both indices. Concerning changes in the snowfall fraction, i.e.,
584 in the relative contribution of snowfall to total precipitation, our results indicate that current seasonal
585 and domain mean S_{frac} might drop by about -50% (Fig. 8, lowermost row). Below 1000 m a.s.l., the
586 strength of the signal is almost independent of the month, and multi-model average changes of the
587 snow fraction of about -80% are obtained. At higher elevations changes during mid-winter are less
588 pronounced compared to autumn and spring but still negative.

589 **5 Discussion**

590 **5.1 Effect of temperature, snowfall frequency and intensity on snowfall changes**

591 The results in Section 4 indicate substantial changes of snowfall indices over the Alps in regional
592 climate projections. With complementary analyses presented in Figures 9 and 10 we shed more light
593 on the responsible mechanisms, especially concerning projected changes in mean and heavy
594 snowfall. For this purpose Figures 9a-b,e-f show the relationship of both mean and heavy snowfall
595 amounts in the CTRL period and their respective percentage changes with the climatological CTRL
596 temperature of the respective (climatological) month, elevation interval and GCM-RCM chain. For
597 absolute amounts (S_{mean} , S_{q99} ; Fig. 9a,e) a clear negative relation is found, i.e., the higher the CTRL
598 temperature the lower the snowfall amounts. For S_{mean} the relation levels off at mean temperatures

599 higher than about 6°C with mean snowfall amounts close to zero. For temperatures below about -6°C
600 a considerable spread in snowfall amounts is obtained, i.e., mean temperature does not seem to be
601 the controlling factor here. Relative changes of both quantities (Fig. 9b,f), however, are strongly
602 controlled by the CTRL period's temperature level with losses close to 100% for warm climatic settings
603 and partly increasing snowfall amounts for colder climates. This dependency of relative snowfall
604 changes on CTRL temperature is in line with previous works addressing future snowfall changes on
605 both hemispheric and regional scales (de Vries et al., 2014; Krasting et al., 2013; Räisänen, 2016).
606 The spread of changes within a given CTRL temperature bin can presumably be explained by the
607 respective warming magnitudes that differ between elevations, months and GCM-RCM chains. About
608 half of this spread can be attributed to the month and the elevation alone (compare the spread of the
609 black markers to the one of the red markers which indicate multi-model averages).

610 For most months and elevation intervals, percentage reductions in S_{mean} and S_{q99} reveal an almost
611 linear relationship with δS_{freq} (Fig. 9c, g). The decrease of S_{freq} with future warming can be explained
612 by a shift of the temperature probability distribution towards higher temperatures, leading to fewer
613 days below the freezing level (Fig. 10, top row). Across the three elevation intervals <1000 m a.s.l.,
614 1000-2000 m a.s.l. and > 2000 m a.s.l., relative changes in the number of days with temperatures
615 below the freezing level ($T \leq 0^\circ\text{C}$) are in the order of -65%, -40% and -20%, respectively (not shown).
616 This approximately corresponds to the simulated decrease of S_{freq} (cf. Fig 8), which in turn, is of a
617 similar magnitude as found in previous works addressing future snowfall changes in the Alps
618 (Schmucki et al., 2015b; Zubler et al., 2014). Due to the general shift of the temperature distribution
619 and the "loss" of very cold days (Fig. 10, top row) future snowfall furthermore occurs in a narrower
620 temperature range (Fig. 10, second row).

621 Contrasting this general pattern of frequency-driven decreases of both mean and heavy snowfall, no
622 changes or even slight increases of S_{mean} , S_{q99} and $S_{1\text{d}}$ at high elevations are expected in mid-winter
623 (see Fig. 8). This can to some part be explained by the general increase of total winter precipitation
624 (Rajczak et al., in prep; Smiatek et al., 2016) that obviously offsets the warming effect in high-elevation
625 regions where a substantial fraction of the future temperature PDF is still located below the rain-snow
626 transition (Fig. 10, top row). This process has also been identified in previous works to be, at last
627 partly, responsible for future snowfall increases (de Vries et al., 2014; Krasting et al., 2013; Räisänen,
628 2016). Furthermore, the magnitude of the increases of both mean and heavy snowfall is obviously
629 driven by positive changes of S_{int} , while S_{freq} remains constant (Fig. 9c,g). An almost linear relationship
630 between positive changes of S_{int} and positive changes of S_{mean} and S_{q99} is obtained (Fig. 9d,h; upper
631 right quadrants. Nevertheless, the high-elevation mid-winter growth in S_{mean} is smaller than the
632 identified increases of mean winter total precipitation. This can be explained by the persistent
633 decrease of S_{frac} during the cold season (see Fig. 8, lowermost row).

634 For elevation intervals with simulated monthly temperatures between -6°C and 0°C in the CTRL
635 period, S_{mean} appears to decrease stronger than S_{q99} (cf. Fig. 9b,f). O'Gorman (2014) found a very
636 similar behaviour when analysing mean and extreme snowfall projections over the Northern
637 Hemisphere within a set of GCMs. This finding is related to the fact that future snowfall decreases are

638 mainly governed by a decrease of snowfall frequency while snowfall increases in high-elevated
639 regions in mid-winter seem to be caused by increases of snowfall intensity. It can obviously be
640 explained by the insensitivity of the temperature interval at which extreme snowfall occurs to climate
641 warming and by the shape of the temperature – snowfall intensity distribution itself (Fig. 10, third row).
642 The likely reason behind positive changes of S_{int} at high-elevated and cold regions is the higher water
643 holding capacity of the atmosphere in a warmer climate. According to the Clausius-Clapeyron relation,
644 saturation vapour pressure increases by about 7% per degree warming (Held and Soden, 2006).
645 Previous studies have shown that simulated changes of heavy and extreme precipitation (though not
646 necessarily targeting the daily temporal scale and moderate extremes as in our case) are consistent
647 with this theory (e.g., Allen and Ingram, 2002; Ban et al., 2015). In terms of snowfall, we find the
648 Clausius-Clapeyron relation to be applicable for negative temperatures up to approximately -5°C as
649 well (Fig. 10, third row, dashed lines). Inconsistencies for temperatures between -5°C and 0°C are due
650 to a snow fraction $sf < 100\%$ for corresponding precipitation events.

651 For further clarification, Figure 11 schematically illustrates the governing processes behind the
652 changes of mean and heavy snowfall that differ between climatologically warm (decreasing snowfall)
653 and climatologically cold climates (increasing snowfall). As shown in Figure 10 (third row), the mean
654 S_{int} distribution is rather independent on future warming and similar temperatures are associated with
655 similar mean snowfall intensities. In particular, heaviest snowfall is expected to occur slightly below the
656 freezing level in both the CTRL and the SCEN period (Fig. 11a). How often do such conditions prevail
657 in the two periods? In a warm current climate, i.e., at low elevations or in the transition seasons, heavy
658 snowfall only rarely occurs as the temperature interval for highest snowfall intensity is already situated
659 in the left tail of the CTRL period's temperature distribution (Fig. 11b). With future warming, i.e., with a
660 shift of the temperature distribution to the right, the probability for days to occur in the heavy snowfall
661 temperature interval (dark grey shading) decreases stronger than the probability of days to occur in
662 the overall snowfall regime (light grey shading). This results in (1) a general decrease of snowfall
663 frequency, (2) a general decrease of mean snowfall intensity and (3) a general and similar decrease of
664 both mean and heavy snowfall amounts. In contrast, at cold and high-elevated sites CTRL period
665 temperatures are often too low to trigger heavy snowfall since a substantial fraction of the temperature
666 PDF is located to the left of the heavy snowfall temperature interval (Fig. 11 c). The shifted distribution
667 in a warmer SCEN climate, however, peaks within the temperature interval that favours heavy
668 snowfall. This leads to a probability increase for days to occur in the heavy snowfall temperature range
669 despite the general reduction in S_{freq} (lower overall probability of days to occur in the entire snowfall
670 regime, light grey). As a consequence, mean S_{int} tends to increase and the reduction of heavy snowfall
671 amounts is less pronounced (or even of opposing sign) than the reduction in mean snowfall. For
672 individual (climatologically cold) regions and seasons, the increase of mean S_{int} might even
673 compensate the S_{freq} decrease, resulting in an increase of both mean and heavy snowfall amounts.
674 Note that in a strict sense these explanations only hold in the case that the probability of snowfall to
675 occur at a given temperature does not change considerably between the CTRL and the SCEN period.
676 This behaviour is approximately found (Fig. 10, bottom row), which presumably indicates only minor
677 contributions of large scale circulation changes and associated humidity changes on both the
678 temperature - snowfall frequency and the temperature - snowfall intensity relation.

679 **5.2 Emission scenario uncertainty**

680 The projections presented in the previous sections are based on the RCP8.5 emission scenario, but
681 will depend on the specific scenario considered. To assess this type of uncertainty we here compare
682 the RCM_{sep+ba} simulations for the previously shown RCP8.5 emission scenario against those assuming
683 the more moderate RCP4.5 scenario. As a general picture, the weaker RCP4.5 scenario is associated
684 with less pronounced changes of snowfall indices (Fig. 12). Differences in mean seasonal δS_{mean}
685 between the two emission scenarios are most pronounced below 1000 m a.s.l. where percentage
686 changes for RCP4.5 are about one third smaller than for RCP8.5. At higher elevations, multi-model
687 mean changes better agree and the multi-model ranges for the two emission scenarios start
688 overlapping, i.e., individual RCP4.5 experiments can be located in the RCP8.5 multi-model range and
689 vice versa. Over the entire Alpine domain, about -25% of current snowfall is expected to be lost under
690 the moderate RCP4.5 emission scenario while a reduction of approximately -45% is projected for
691 RCP8.5. For seasonal cycles, the difference of δS_{mean} between RCP4.5 and RCP8.5 is similar for
692 most months and slightly decreases with altitude. Above 2000 m a.s.l., the simulated increase of S_{mean}
693 appears to be independent of the chosen RCP in January and February, while negative changes
694 before and after mid-winter are more pronounced for RCP8.5. Alpine domain mean δS_{q99} almost
695 doubles under the assumption of stronger GHG emissions. This is mainly due to differences at low
696 elevations whereas above 2000 m a.s.l. δS_{q99} does not seem to be strongly affected by the choice of
697 the emission scenario. Differences in monthly mean changes are in close analogy to δS_{mean} . Higher
698 emissions lead to a further negative shift in δS_{q99} . Up to mid-elevations differences are rather
699 independent of the season. However, at highest elevations and from January to March, differences
700 between RCP4.5 and RCP8.5 are very small.

701 Despite the close agreement of mid-winter snowfall increases at high elevations between the two
702 emission scenarios, obvious differences in the spatial extent of the region of mean seasonal snowfall
703 increases can be found (cf Figs. S6 and 7 for δS_{mean} , and Figs. S7 and S8 for δS_{q99}). In most
704 simulations, the number of grid cells along the main Alpine ridge that show either little change or even
705 increases of seasonal mean S_{mean} or S_{q99} is larger for RCP4.5 than for RCP8.5 with its larger warming
706 magnitude.

707 **5.3 Intercomparison of projections with separated and raw snowfall**

708 The snowfall projections presented above are based on the RCM_{sep+ba} data set, i.e. on separated and
709 bias-adjusted snowfall amounts. To assess the robustness of these estimates we here compare the
710 obtained change signals against the respective signals based on $RCM_{sep+nba}$ (separated and not bias-
711 adjusted) and simulated raw snowfall output (RCM_{raw}). This comparison is restricted to the nine RCMs
712 providing raw snowfall as output variable (see Tab. 1).

713 The three different change estimates agree well with each other In terms of relative snowfall change
714 signals (Fig. 13, top row). Multi-model mean relative changes are very similar for all analysed snowfall
715 indices and elevation intervals. In many cases, separated and not bias-adjusted snowfall ($RCM_{sep+nba}$)
716 is subject to slightly smaller percentage decreases. Multi-model mean differences between RCM_{sep+ba} ,
717 $RCM_{sep+nba}$ and RCM_{raw} simulations are smaller than the corresponding multi-model spread of

718 RCM_{sep+ba} simulations and emission scenario uncertainties (cf. Figs. 12, 13 and S10). This agreement
719 in terms of relative change signals is in contrast to absolute change characteristics (Fig. 13, bottom
720 row). Results based on the three data sets agree in the sign of change, but not in their magnitude,
721 especially at high elevations >2000 m a.s.l.. As the relative changes are almost identical, the absolute
722 changes strongly depend upon the treatment of biases in the control climate.

723 In summary, these findings indicate that (a) the snowfall separation method developed in the present
724 work yields rather good proxies for relative changes of snowfall indices in raw RCM output (which is
725 not available for all GCM-RCM chains), and that (b) the additional bias adjustment of separated
726 snowfall amounts only has a weak influence on relative change signals of snowfall indices, but can
727 have substantial effects on absolute changes.

728 **6 Conclusions and outlook**

729 The present work makes use of state-of-the-art EURO-CORDEX RCM simulations to assess changes
730 of snowfall indices over the European Alps by the end of the 21st century. For this purpose, snowfall is
731 separated from total precipitation using near-surface air temperature in both the RCMs and in the an
732 observation-based estimate on a daily basis. The analysis yields a number of robust signals,
733 consistent across a range of climate model chains and across emission scenarios. Relating to the
734 main objectives we find the following:

735 **Snowfall separation on an RCM grid.** Binary snow fractionation with a fixed temperature threshold
736 on coarse-resolution grids (with 11 km resolution) leads to an underestimation of mean snowfall and
737 an overestimation of heavy snowfall. To overcome these deficiencies, the Richards snow fractionation
738 method is implemented. This approach expresses that the coarse-grid snow fraction depends not only
739 on daily mean temperature, but also on topographical subgrid-scale variations. Accounting for the
740 latter results in better estimates for mean and heavy snowfall. However, due to limited observational
741 coverage the parameters of this method are fitted for Switzerland only and are then applied to the
742 entire Alpine domain. Whether this spatial transfer is robust could further be investigated by using
743 observational data sets covering the full domain of interest but is out of the scope of this study.

744 **Snowfall bias adjustment.** Simulations of the current EURO-CORDEX ensemble are subject to
745 considerable biases in precipitation and temperature, which translate into biased snowfall amounts. In
746 the EVAL period, simulated precipitation is largely overestimated, with increasing biases toward higher
747 altitudes. On the other hand, simulated near surface temperatures are generally too low with largest
748 deviations over mountainous regions. These findings were already reported in previous studies for
749 both the current EURO-CORDEX data set but also for previous RCM ensembles (e.g. Frei et al., 2003;
750 Kotlarski et al., 2012; Kotlarski et al., 2015; Rajczak et al., 2013; Smiatek et al., 2016). By
751 implementing a simple bias adjustment approach, we are able to partly reduce these biases and the
752 associated model spread, which should enable more robust change estimates. The adjusted model
753 results reproduce the seasonal cycles of mean snowfall fairly well. However, substantial biases remain
754 in terms of heavy snowfall, snowfall intensities (which in general are overestimated), snowfall
755 frequencies, and spatial snowfall distributions. Further improvements might be feasible by using more

756 sophisticated bias adjustment methods, such as quantile mapping (e.g., Rajczak et al., 2016), local
757 intensity scaling of precipitation (e.g., Schmidli et al., 2006), or weather generators (e.g. Keller et al.,
758 2016). Advantages of the approach employed here are its simplicity, its direct linkage to the snowfall
759 separation method and, as a consequence, its potential ability to account for non-stationary snowfall
760 biases. Furthermore, a comparison to simulated raw snowfall for a subset of nine simulations revealed
761 that relative change signals are almost independent of the chosen post-processing strategy.

762 **Snowfall projections for the late 21st century.** Snowfall climate change signals are assessed by
763 deriving the changes in snowfall indices between the CTRL period 1981 - 2010 and the SCEN period
764 2070 - 2099. Our results show that by the end of the 21st century, snowfall over the Alps will be
765 considerably reduced. Between September and May mean snowfall is expected to decrease by
766 approximately -45% (multi-model mean) under an RCP8.5 emission scenario. For the more moderate
767 RCP4.5 scenario, multi-model mean projections show a decline of -25%. These results are in good
768 agreement with previous works (e.g. de Vries et al., 2014; Piazza et al., 2014, Räisänen, 2016). Low-
769 lying areas experience the largest percentage changes of more than -80%, while the highest Alpine
770 regions are only weakly affected. Variations of heavy snowfall, defined by the 99% all-day snowfall
771 percentile, show an even more pronounced signal at low-lying elevations. With increasing elevation,
772 percentage changes of heavy snowfall are generally smaller than for mean snowfall. O'Gorman (2014)
773 found a very similar behaviour by analysing projected changes in mean and extreme snowfall over the
774 entire Northern Hemisphere. He pointed out that heavy and extreme snowfall occurs near an optimal
775 temperature (near or below freezing, but not too cold), which seems to be independent of climate
776 warming. We here confirm this finding. At mid and high elevations heavy snowfall in a warmer climate
777 will still occur in the optimal temperature range, hence, heavy snowfall amounts will decrease less
778 strongly compared to mean snowfall, and may even increase in some areas.

779 At first approximation, the magnitude of future warming strongly influences the reduction of mean and
780 heavy snowfall by modifying the snowfall frequency. Snowfall increases may however occur at high
781 (and thus cold) elevations, and these are not caused by frequency changes. Here, snowfall increases
782 due to (a) a general increase of total winter precipitation combined with only minor changes in snowfall
783 frequency, and (b) more intense snowfall. This effect has a pronounced altitudinal distribution and may
784 be particularly strong under conditions (depending upon location and season) where the current
785 climate is well below freezing. Such conditions may experience a shift towards a temperature range
786 more favourable to snowfall (near or below freezing, but not too cold) with corresponding increases of
787 mean snowfall, despite a general decrease of the snowfall fraction.

788 The identified future changes of snowfall over the Alps can lead to a variety of impacts in different
789 sectors. With decreasing snowfall frequencies and the general increase of the snowline (e.g.,
790 Beniston, 2003; Gobiet et al., 2014; Hantel et al., 2012), both associated with temperature changes,
791 ski lift operators are looking into an uncertain future. A shorter snowfall season will likely put them
792 under greater financial pressure. Climate change effects might be manageable only for ski areas
793 reaching up to high elevations (e.g. Elsasser and Bürki, 2002). Even so these resorts might start later
794 into the ski season, the snow conditions into early spring could change less dramatically due to

795 projected high-elevation snowfall increases in mid-winter. A positive aspect of the projected decrease
796 in snowfall frequency might be a reduced expenditures for airport and road safety (e.g., Zubler et al.,
797 2015).

798 At lower altitudes, an intensification of winter precipitation, combined with smaller snowfall fractions
799 (Serquet et al., 2013), increases the flood potential (Beniston, 2012). Snow can act as a buffer by
800 releasing melt water constantly over a longer period of time. With climate warming, this storage
801 capacity is lost, and heavy precipitation immediately drains into streams and rivers which might not be
802 able to take up the vast amount of water fast enough. Less snowmelt will also have impacts on
803 hydropower generation and water management (e.g., Weingartner et al., 2013). So far, many Alpine
804 regions are able to bypass dry periods by tapping melt water from mountainous regions. With reduced
805 snow-packs due to less snowfall, water shortage might become a serious problem in some areas.

806 Regarding specific socio-economic impacts caused by extreme snowfall events, conclusions based on
807 the results presented in this study are difficult to draw. It might be possible that the 99% all-day
808 snowfall percentile we used for defining heavy snowfalls, is not appropriate to speculate about future
809 evolutions of (very) rare events (Schär et al., 2016). To do so, one might consider applying a
810 generalized extreme value (GEV) analysis which is more suitable for answering questions related to
811 rare extreme events.

812 **7 Data Availability**

813 The EURO-CORDEX RCM data analysed in the present work are publicly available - parts of
814 them for non-commercial use only - via the Earth System Grid Federation archive (ESGF;
815 e.g., <https://esgf-data.dkrz.de>). The observational datasets RHiresD and TabsD as well as
816 the snow depth data for Switzerland are available for research and educational purposes
817 from kundendienst@meteoschweiz.ch. The analysis code is available from the
818 corresponding author on request.

819 **8 Competing Interests**

820 The authors declare that they have no conflict of interest.

821 **9 Acknowledgements**

822 We gratefully acknowledge the support of Jan Rajczak, Urs Beyerle and Curdin Spirig (ETH Zurich) as
823 well as Elias Zubler (MeteoSwiss) in data acquisition and pre-processing. Christoph Frei (MeteoSwiss)
824 and Christoph Marty (WSL-SLF) provided important input on specific aspects of the analysis. The
825 GTOPO30 digital elevation model is available from the U.S. Geological Survey. Finally, we thank the
826 climate modelling groups of the EURO-CORDEX initiative for producing and making available their
827 model output.

828 **10 References**

- 829 Abegg, B. A., S., Crick, F., and de Montfalcon, A.: Climate change impacts and adaptation in winter tourism, in:
830 Climate change in the European Alps: adapting winter tourism and natural hazards management, edited by:
831 Agrawala, S., Organisation for Economic Cooperation and Development (OECD), Paris, France, 25-125, 2007.
- 832 Allen, M. R., and Ingram, W. J.: Constraints on future changes in climate and the hydrologic cycle, *Nature*, 419,
833 224-232, 10.1038/nature01092, 2002.
- 834 Ban, N., Schmidli, J., and Schär, C.: Heavy precipitation in a changing climate: Does short-term summer
835 precipitation increase faster?, *Geophys Res Lett*, 42, 1165-1172, 10.1002/2014GL062588, 2015.
- 836 Beniston, M.: Climatic Change in Mountain Regions: A Review of Possible Impacts. *Clim Change*, 59, 5-31.
- 837 Beniston, M.: Impacts of climatic change on water and associated economic activities in the Swiss Alps, *J Hydrol*,
838 412, 291-296, 10.1016/j.jhydrol.2010.06.046, 2012.
- 839 Ceppi, P., Scherrer, S.C., Fischer, A.M., and Appenzeller, C.: Revisiting Swiss temperature trends 1959–2008, *Int
840 J Climatol*, 32, 203-213, 10.1002/joc.2260, 2012.
- 841 CH2011: Swiss Climate Change Scenarios CH2011, published by C2SM, MeteoSwiss, ETH, NCCR Climate, and
842 OcCC, Zurich, Switzerland, 88 pp, 2011.
- 843 Chimani, B., Böhm, R., Matulla, C., and Ganekind, M.: Development of a longterm dataset of solid/liquid
844 precipitation, *Adv Sci Res*, 6, 39-43, 10.5194/asr-6-39-2011, 2011.
- 845 de Vries, H., Haarsma, R. J., Hazeleger, W.: On the future reduction of snowfall in western and central Europe.
846 *Clim Dyn*, 41, 2319-2330, 10.1007/s00382-012-1583-x, 2013.
- 847 de Vries, H., Lenderink, G., and van Meijgaard, E.: Future snowfall in western and central Europe projected with a
848 high-resolution regional climate model ensemble, *Geophys Res Lett*, 41, 4294-4299, 10.1002/2014GL059724,
849 2014.
- 850 Deser, C., Knutti, R., Solomon, S. and Phillips, A. S.: Communication of the role of natural variability in future
851 North American climate. *Nature Clim Change*, 2, 775-779, 2012.
- 852 Elsasser, H. and Bürki, R.: Climate change as a threat to tourism in the Alps. *Climate Research*, 20, 253-257.
- 853 Fischer, A. M., Keller, D. E., Liniger, M. A., Rajczak, J., Schär, C., and Appenzeller, C.: Projected changes in
854 precipitation intensity and frequency in Switzerland: a multi-model perspective, *Int J Climatol*, 35, 3204-3219,
855 10.1002/joc.4162, 2015.
- 856 Fischer, E. M. and Knutti, R.: Observed heavy precipitation increase confirms theory and early models. *Nature
857 Clim Change*, 6, 986-992, 10.1038/NCLIMATE3110, 2016.
- 858 Frei, C. and Schär, C.: A precipitation climatology of the Alps from high-resolution rain-gauge observations, *Int J
859 Climatol*, 18, 873-900, 10.1002/(Sici)1097-0088(19980630)18:8<873::Aid-Joc255>3.0.Co;2-9, 1998.
- 860 Frei, C., Christensen, J. H., Déqué, M., Jacob, D., Jones, R. G., and Vidale, P. L.: Daily precipitation statistics in
861 regional climate models: Evaluation and intercomparison for the European Alps, *J Geophys Res-Atmos*, 108,
862 10.1029/2002jd002287, 2003.
- 863 Frei, C.: Interpolation of temperature in a mountainous region using nonlinear profiles and non-Euclidean
864 distances, *Int J Climatol*, 34, 1585-1605, 10.1002/joc.3786, 2014.
- 865 Giorgi, F.: Simulation of regional climate using a limited area model nested in a general circulation model, *J
866 Climate*, 3, 941-963, 1990.
- 867 Giorgi, F., Jones, C., and Asrar, G. R.: Addressing climate information needs at the regional level: the CORDEX
868 framework, *World Meteorological Organization (WMO) Bulletin*, 58, 175, 2009.
- 869 Giorgi, F., Torma, C., Coppola, E., Ban, N., Schär, C., and Somot, S.: Enhanced summer convective rainfall at
870 Alpine high elevations in response to climate warming, *Nat Geo*, 9, 584-589, 10.1038/ngeo2761, 2016.
- 871 Gobiet, A., Kotlarski, S., Beniston, M., Heinrich, G., Rajczak, J., and Stoffel, M.: 21st century climate change in
872 the European Alps - A review, *Science of the Total Environment*, 493, 1138-1151,
873 10.1016/j.scitotenv.2013.07.050, 2014.
- 874 Grünewald, T., and Lehning, M.: Are flat-field snow depth measurements representative? A comparison of
875 selected index sites with areal snow depth measurements at the small catchment scale, *Hydrol Processes*, 29,
876 1717-1728, 10.1002/hyp.10295, 2015.
- 877 Hantel, M., Maurer, C., and Mayer, D.: The snowline climate of the Alps 1961–2010. *Theor Appl Climatol*, 110,
878 517, 10.1007/s00704-012-0688-9, 2012.
- 879 Hawkins, E., and Sutton, R.: The Potential to Narrow Uncertainty in Regional Climate Predictions, *B Am Meteorol
880 Soc*, 90, 1095+, 10.1175/2009BAMS2607.1, 2009.

881 Haylock, M.R., Hofstra, N., Klein Tank, A.M.G., Klok, E.J., Jones, P.D., and New, M.: A European daily high-
882 resolution gridded data set of surface temperature and precipitation for 1950–2006, *J Geophys Res*, 113,
883 D20119, 10.1029/2008JD010201.

884 Held, I. M., and Soden, B. J.: Robust responses of the hydrological cycle to global warming, *J Climate*, 19, 5686-
885 5699, 10.1175/Jcli3990.1, 2006.

886 IPCC: Climate Change 2013: The Physical Science Basis. Contribution of Working Group I to the Fifth
887 Assessment Report of the Intergovernmental Panel on Climate Change, Cambridge University Press, Cambridge,
888 United Kingdom and New York, NY, USA, 1535 pp., 2013.

889 Isotta, F. A., Frei, C., Weilguni, V., Tadic, M. P., Lassegues, P., Rudolf, B., Pavan, V., Cacciamani, C., Antolini,
890 G., Ratto, S. M., Munari, M., Micheletti, S., Bonati, V., Lussana, C., Ronchi, C., Panettieri, E., Marigo, G., and
891 Vertacnik, G.: The climate of daily precipitation in the Alps: development and analysis of a high-resolution grid
892 dataset from pan-Alpine rain-gauge data, *Int J Climatol*, 34, 1657-1675, 10.1002/joc.3794, 2014.

893 Jacob, D., Petersen, J., Eggert, B., Alias, A., Christensen, O. B., Bouwer, L. M., Braun, A., Colette, A., Déqué, M.,
894 Georgievski, G., Georgopoulou, E., Gobiet, A., Menut, L., Nikulin, G., Haensler, A., Hempelmann, N., Jones, C.,
895 Keuler, K., Kovats, S., Kröner, N., Kotlarski, S., Kriegsman, A., Martin, E., van Meijgaard, E., Moseley, C.,
896 Pfeifer, S., Preuschmann, S., Radermacher, C., Radtke, K., Rechid, D., Rounsevell, M., Samuelsson, P., Somot,
897 S., Soussana, J. F., Teichmann, C., Valentini, R., Vautard, R., Weber, B., and Yiou, P.: EURO-CORDEX: new
898 high-resolution climate change projections for European impact research, *Reg Environ Change*, 14, 563-578,
899 10.1007/s10113-013-0499-2, 2014.

900 Keller, D. E., Fischer, A. M., Liniger, M. A., Appenzeller, C. and Knutti, R.: Testing a weather generator for
901 downscaling climate change projections over Switzerland. *Int J Climatol*, doi:10.1002/joc.4750, 2016.

902 Kienzle, S. W.: A new temperature based method to separate rain and snow, *Hydrol Process*, 22, 5067-5085,
903 10.1002/hyp.7131, 2008.

904 Kotlarski, S., Bosshard, T., Lüthi, D., Pall, P., and Schär, C.: Elevation gradients of European climate change in
905 the regional climate model COSMO-CLM. *Clim Change*, 112, 189-215, 10.1007/s10584-011-0195-5, 2012.

906 Kotlarski, S., Keuler, K., Christensen, O. B., Colette, A., Deque, M., Gobiet, A., Goergen, K., Jacob, D., Luthi, D.,
907 van Meijgaard, E., Nikulin, G., Schar, C., Teichmann, C., Vautard, R., Warrach-Sagi, K., and Wulfmeyer, V.:
908 Regional climate modeling on European scales: a joint standard evaluation of the EURO-CORDEX RCM
909 ensemble, *Geosci Model Dev*, 7, 1297-1333, 10.5194/gmd-7-1297-2014, 2014.

910 Kotlarski, S., Lüthi, D., and Schär, C.: The elevation dependency of 21st century European climate change: an
911 RCM ensemble perspective, *Int J Climatol*, 35, 3902-3920, 10.1002/joc.4254, 2015.

912 Krasting, J. P., Broccoli, A. J., Dixon, K. W., and Lanzante, J. R.: Future Changes in Northern Hemisphere
913 Snowfall. *J Clim*, 26, 7813-7828, 10.1175/JCLI-D-12-00832.1, 2013.

914 Laternser, M., and Schneebeli, M.: Long-term snow climate trends of the Swiss Alps (1931-99), *Int J Climatol*, 23,
915 733-750, 10.1002/joc.912, 2003.

916 Marty, C.: Regime shift of snow days in Switzerland, *Geophys Res Lett*, 35, 10.1029/2008gl033998, 2008.

917 Marty, C., and Blanchet, J.: Long-term changes in annual maximum snow depth and snowfall in Switzerland
918 based on extreme value statistics, *Climatic Change*, 111, 705-721, 2011.

919 McAfee, S. A., Walsh, J., and Rupp, T. S.: Statistically downscaled projections of snow/rain partitioning for
920 Alaska, *Hydrol Process*, 28, 3930-3946, 10.1002/hyp.9934, 2014.

921 MeteoSchweiz: Klimareport 2015. Bundesamt für Meteorologie und Klimatologie MeteoSchweiz, Zürich.

922 MeteoSwiss: Daily Precipitation (final analysis): RhiresD:
923 www.meteoswiss.admin.ch/content/dam/meteoswiss/de/service-und-publikationen/produkt/raeumliche-daten-
924 niederschlag/doc/ProdDoc_RhiresD.pdf, access: 10.01.2017, 2013a.

925 MeteoSwiss: Daily Mean, Minimum and Maximum Temperature: TabsD, TminD ,TmaxD:
926 www.meteoswiss.admin.ch/content/dam/meteoswiss/de/service-und-publikationen/produkt/raeumliche-daten-
927 temperatur/doc/ProdDoc_TabsD.pdf, access: 10.01.2017, 2013b.

928 Moss, R. H., Edmonds, J. A., Hibbard, K. A., Manning, M. R., Rose, S. K., van Vuuren, D. P., Carter, T. R., Emori,
929 S., Kainuma, M., Kram, T., Meehl, G. A., Mitchell, J. F. B., Nakicenovic, N., Riahi, K., Smith, S. J., Stouffer, R. J.,
930 Thomson, A. M., Weyant, J. P., and Wilbanks, T. J.: The next generation of scenarios for climate change research
931 and assessment, *Nature*, 463, 747-756, 10.1038/nature08823, 2010.

932 Neff, E. L.: How Much Rain Does a Rain Gauge Gauge, *J Hydrol*, 35, 213-220, 10.1016/0022-1694(77)90001-4,
933 1977.

934 O'Gorman, P. A.: Contrasting responses of mean and extreme snowfall to climate change, *Nature*, 512, 416-
935 U401, 10.1038/nature13625, 2014.

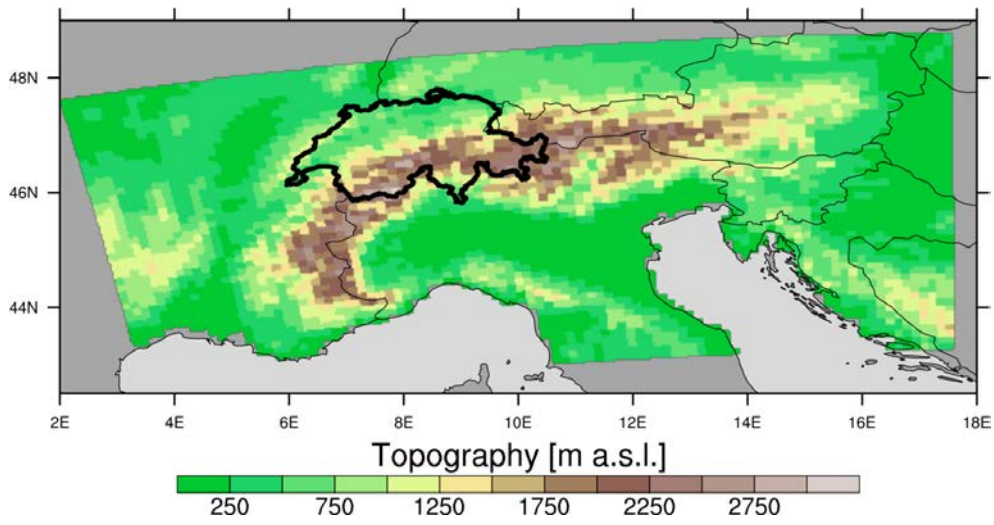
- 936 Piazza, M., Boé, J., Terray, L., Pagé, C., Sanchez-Gomez, E., and Déqué, M.: Projected 21st century snowfall
937 changes over the French Alps and related uncertainties, *Climatic Change*, 122, 583-594, 10.1007/s10584-013-
938 1017-8, 2014.
- 939 Räisänen, J.: Twenty-first century changes in snowfall climate in Northern Europe in ENSEMBLES regional
940 climate models, *Clim Dynam*, 46, 339-353, 10.1007/s00382-015-2587-0, 2016.
- 941 Rajczak, J., Pall, P., and Schär, C.: Projections of extreme precipitation events in regional climate simulations for
942 Europe and the Alpine Region, *J Geophys Res-Atmos*, 118, 3610-3626, 10.1002/jgrd.50297, 2013.
- 943 Rajczak, J., Kotlarski, S., and Schär, C.: Does Quantile Mapping of Simulated Precipitation Correct for Biases in
944 Transition Probabilities and Spell Lengths?, *J Climate*, 29, 1605-1615, 10.1175/Jcli-D-15-0162.1, 2016.
- 945 Rajczak, J. and Schär, C.: Projections of future precipitation extremes over Europe: A multi-model assessment of
946 climate simulations. In preparation.
- 947 Richards, F. J.: A Flexible Growth Function for Empirical Use, *J Exp Bot*, 10, 290-300, 10.1093/Jxb/10.2.290,
948 1959.
- 949 Rummukainen, M.: State-of-the-art with regional climate models, *Wiley Interdisciplinary Reviews-Climate Change*,
950 1, 82-96, 10.1002/wcc.8, 2010.
- 951 Schär, C., Ban, N., Fischer, E. M., Rajczak, J., Schmidli, J., Frei, C., Giorgi, F., Karl, T. R., Kendon, E. J., Tank, A.
952 M. G. K., O'Gorman, P. A., Sillmann, J., Zhang, X. B., and Zwiers, F. W.: Percentile indices for assessing changes
953 in heavy precipitation events, *Climatic Change*, 137, 201-216, 10.1007/s10584-016-1669-2, 2016.
- 954 Scherrer, S. C., Appenzeller, C., and Laternser, M.: Trends in Swiss Alpine snow days: The role of local- and
955 large-scale climate variability, *Geophys Res Lett*, 31, 10.1029/2004gl020255, 2004.
- 956 Schmidli, J., Frei, C., and Vidale, P. L.: Downscaling from GCM precipitation: A benchmark for dynamical and
957 statistical downscaling methods, *Int J Climatol*, 26, 679-689, 10.1002/joc.1287, 2006.
- 958 Schmucki, E., Marty, C., Fierz, C., and Lehning, M.: Simulations of 21st century snow response to climate change
959 in Switzerland from a set of RCMs, *Int J Climatol*, 35, 3262-3273, 10.1002/joc.4205, 2015a.
- 960 Schmucki, E., Marty, C., Fierz, C., Weingartner, R. and Lehning, M.: Impact of climate change in Switzerland on
961 socioeconomic snow indices, *Theor Appl Climatol*, in press, 10.1007/s00704-015-1676-7, 2015b.
- 962 Serquet, G., Marty, C., and Rebetez, M.: Monthly trends and the corresponding altitudinal shift in the
963 snowfall/precipitation day ratio, *Theor Appl Climatol*, 114, 437-444, 10.1007/s00704-013-0847-7, 2013. Sevruck, B.:
964 Der Niederschlag in der Schweiz, Geographisches Institut der Eidgenössischen Technischen Hochschule in
965 Zürich, Abteilung Hydrologie, Zurich, Switzerland, 1985.
- 966 SFOE, Hydropower: <http://www.bfe.admin.ch/themen/00490/00491/index.html?lang=en>, access: 16.09.2016,
967 2014.
- 968 Smiatek, G., Kunstmann, H., and Senatore, A.: EURO-CORDEX regional climate model analysis for the Greater
969 Alpine Region: Performance and expected future change, *J Geophys Res-Atmos*, 121, 7710-7728,
970 10.1002/2015JD024727, 2016.
- 971 Soncini, A., and Bocchiola, D.: Assessment of future snowfall regimes within the Italian Alps using general
972 circulation models, *Cold Reg Sci Technol*, 68, 113-123, 10.1016/j.coldregions.2011.06.011, 2011.
- 973 Steger, C., Kotlarski, S., Jonas, T., and Schär, C.: Alpine snow cover in a changing climate: a regional climate
974 model perspective, *Clim Dynam*, 41, 735-754, 10.1007/s00382-012-1545-3, 2013.
- 975 Techel, F., Stucki, T., Margreth, S., Marty, C., and Winkler, K.: Schnee und Lawinen in den Schweizer Alpen.
976 Hydrologisches Jahr 2013/14, WSL-Institut für Schnee- und Lawinenforschung SLF, Birmensdorf, Switzerland,
977 2015.
- 978 Terzago, S., von Hardenberg, J., Palazzi, E., and Provenzale, A.: Snow water equivalent in the Alps as seen by
979 gridded datasets, CMIP5 and CORDEX climate models. *The Cryosphere Discussion*, 10.5194/tc-2016-280, 2017.
- 980 Torma, C., Giorgi, F., and Coppola, E.: Added value of regional climate modeling over areas characterized by
981 complex terrain Precipitation over the Alps, *J Geophys Res-Atmos*, 120, 3957-3972, 10.1002/2014JD022781,
982 2015.
- 983 Vautard, R., Gobiet, A., Jacob, D., Belda, M., Colette, A., Déqué, M., Fernandez, J., Garcia-Diez, M., Goergen,
984 K., Guttler, I., Halenka, T., Karacostas, T., Katragkou, E., Keuler, K., Kotlarski, S., Mayer, S., van Meijgaard, E.,
985 Nikulin, G., Patarcic, M., Scinocca, J., Sobolowski, S., Suklitsch, M., Teichmann, C., Warrach-Sagi, K.,
986 Wulfmeyer, V., and Yiou, P.: The simulation of European heat waves from an ensemble of regional climate
987 models within the EURO-CORDEX project, *Clim Dynam*, 41, 2555-2575, 10.1007/s00382-013-1714-z, 2013.
- 988 Weingartner, R., Schädler, B., and Hägggi, P.: Auswirkungen der Klimaänderung auf die schweizerische
989 Wasserkraftnutzung, *Geographica Helvetica*, 68, 239-248, 2013.

- 990 Yang, D. Q., Elomaa, E., Tuominen, A., Aaltonen, A., Goodison, B., Gunther, T., Golubev, V., Sevruk, B.,
991 Madsen, H., and Milkovic, J.: Wind-induced precipitation undercatch of the Hellmann gauges, *Nord Hydrol*, 30,
992 57-80, 1999.
- 993 Zubler, E. M., Scherrer, S. C., Croci-Maspoli, M., Liniger, M. A., and Appenzeller, C.: Key climate indices in
994 Switzerland; expected changes in a future climate, *Climatic Change*, 123, 255-271, 10.1007/s10584-013-1041-8,
995 2014.
- 996 Zubler, E. M., Fischer, A. M., Liniger, M. A., and Schlegel, T.: Auftausalzverbrauch im Klimawandel, MeteoSwiss,
997 Zurich, Switzerland, Fachbericht 253, 2015.
- 998

999 **Figures**

1000

1001

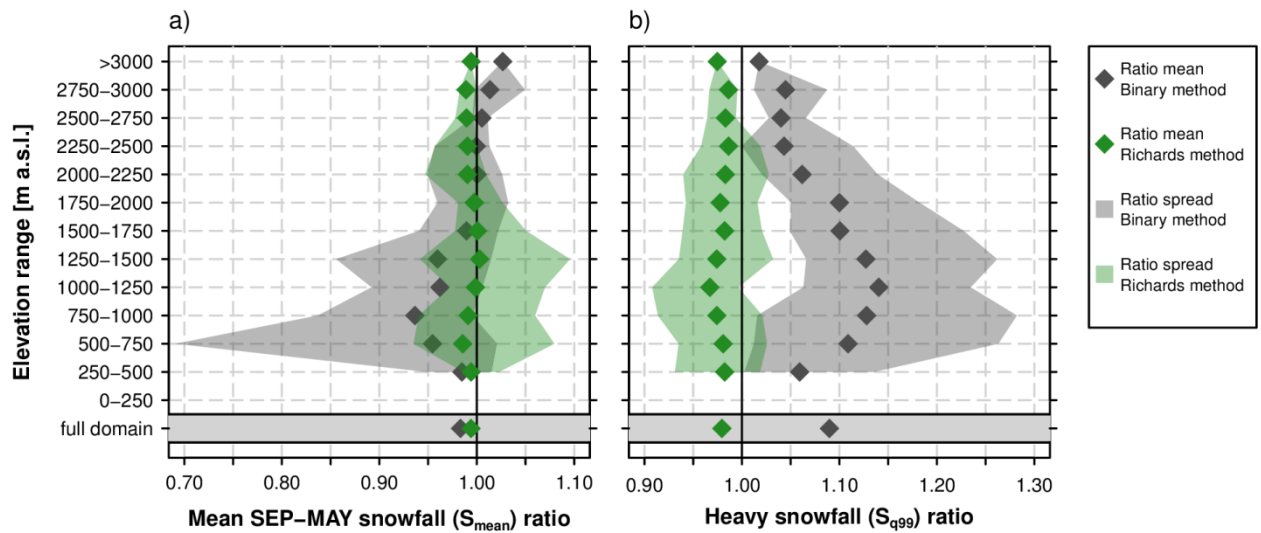


1002

1003

1004 **Figure 1** GTOPO30 topography (<https://ta.cr.usgs.gov/GTOPO30>) aggregated to the EUR-11 (0.11°) RCM grid.
1005 The coloured area shows the Alpine domain used for the assessment of snowfall projections. The bold black
1006 outline marks the Swiss sub-domain used for the assessment of the bias adjustment approach.

1007

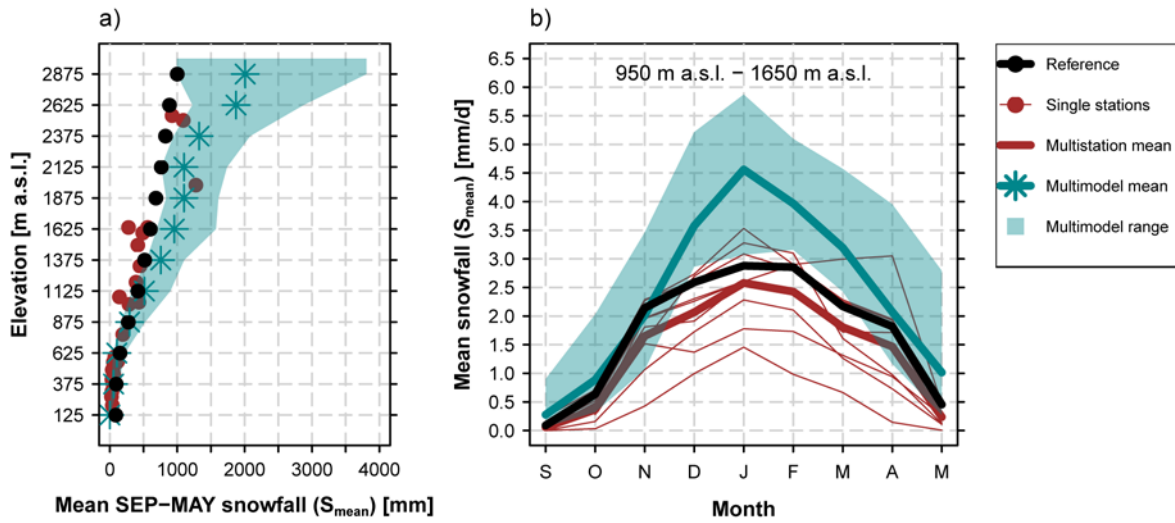


1008
1009

1010 **Figure 2** Snowfall ratios for the Binary and Richards snow fractionation method (ratio between the snowfall of the
 1011 respective method and the *Subgrid* method). The ratios are valid at the coarse-resolution grid (12 km). a) Ratios
 1012 for mean snowfall, S_{mean} . b) Ratios for heavy snowfall, S_{q99} . Ratio means were derived after averaging the
 1013 corresponding snowfall index for 250 m elevation intervals in Switzerland while the ratio spread represents the
 1014 minimum and maximum grid point-based ratios in the corresponding elevation interval. This analysis is entirely
 1015 based on the observational data sets TabsD and RhiresD.

1016

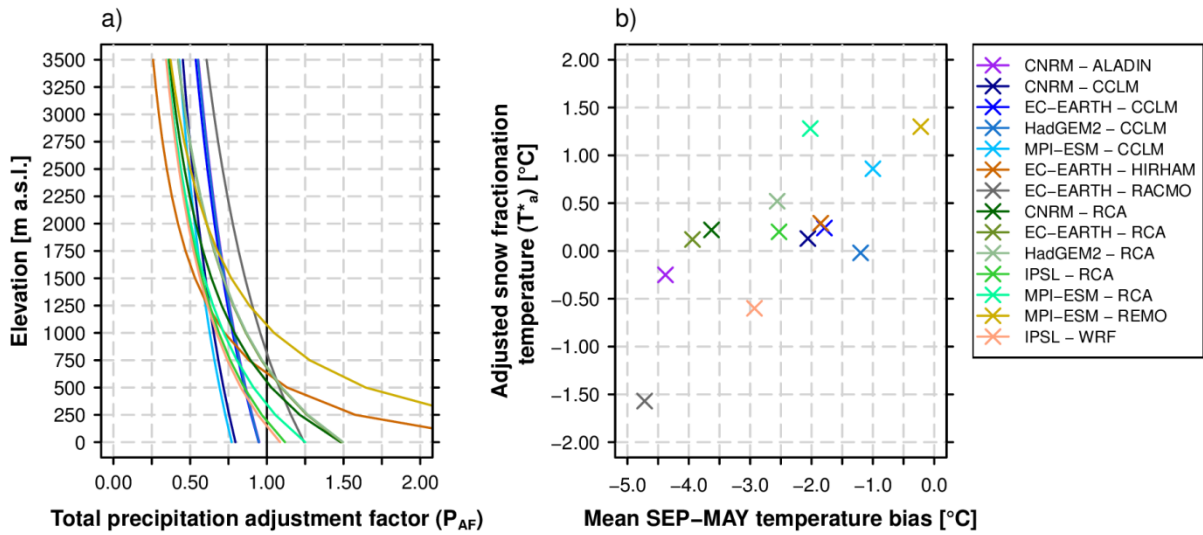
1017



1018

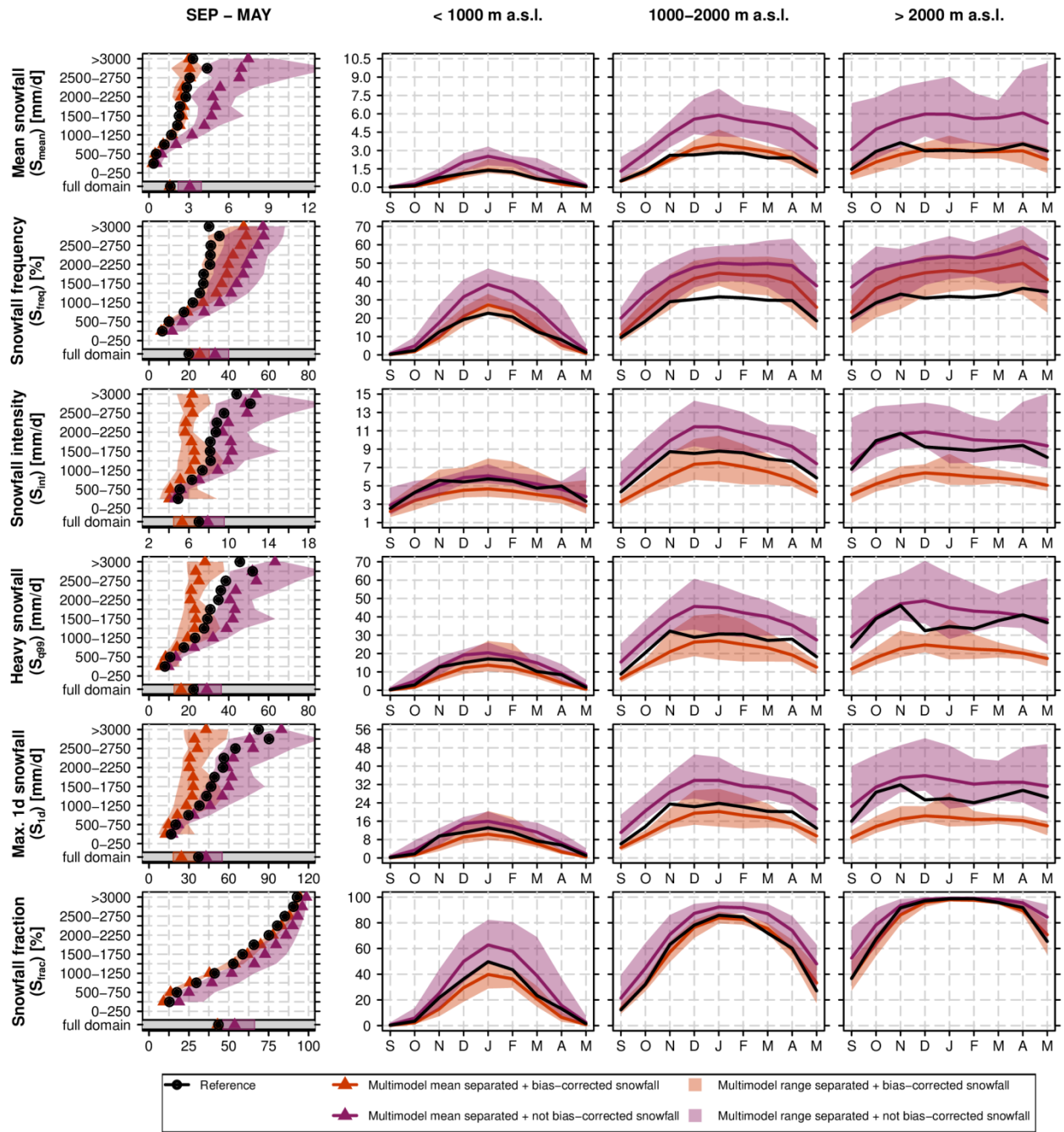
1019 **Figure 3** Comparison of measured fresh snow sums of 29 MeteoSwiss stations (red) against simulated RCM raw
1020 snowfall in Switzerland (green) and against the 2 km reference snowfall grid obtained by employing the *Subgrid*
1021 *method* (black) in the EVAL period 1971-2005. a) Mean September – May snowfall vs. elevation. Both the
1022 simulation data (green) and the reference data (black) are based on the spatio-temporal mean of 250 m elevation
1023 ranges and plotted at the mean elevation of the corresponding interval. b) Seasonal September-May snowfall
1024 cycle for the elevation interval 950 m a.s.l. to 1650 m a.s.l.. Simulated multi-model means and spreads are based
1025 on a subset of 9 EURO-CORDEX simulations providing raw snowfall as output variable (see Tab. 1).

1026



1027
1028

1029 **Figure 4** Overview on bias adjustment. a) Elevation-dependent total precipitation adjustment factors, P_{AF} , for the
 1030 14 GCM-RCM chains (see Eq. 10). b) Scatterplot of mean September to May temperature biases (RCM
 1031 simulation minus observational analysis) vs. adjusted snow fractionation temperatures, T_a^* .



1032
1033

1034 **Figure 5** Evaluation of snowfall indices in the EVAL period 1971-2005 for the 14 snowfall separated + bias-
 1035 adjusted (RCM_{sep+ba}) and 14 snowfall separated + not bias-adjusted ($RCM_{sep+nba}$) RCM simulations vs.
 1036 observation-based reference. The first column shows the mean September-May snowfall index statistics vs.
 1037 elevation while the monthly snowfall indices (spatially averaged over the elevation intervals <1000 m.a.s.l., 1000
 1038 m a.s.l.-2000 m a.s.l. and >2000 m a.s.l.) are displayed in columns 2-4.

1039

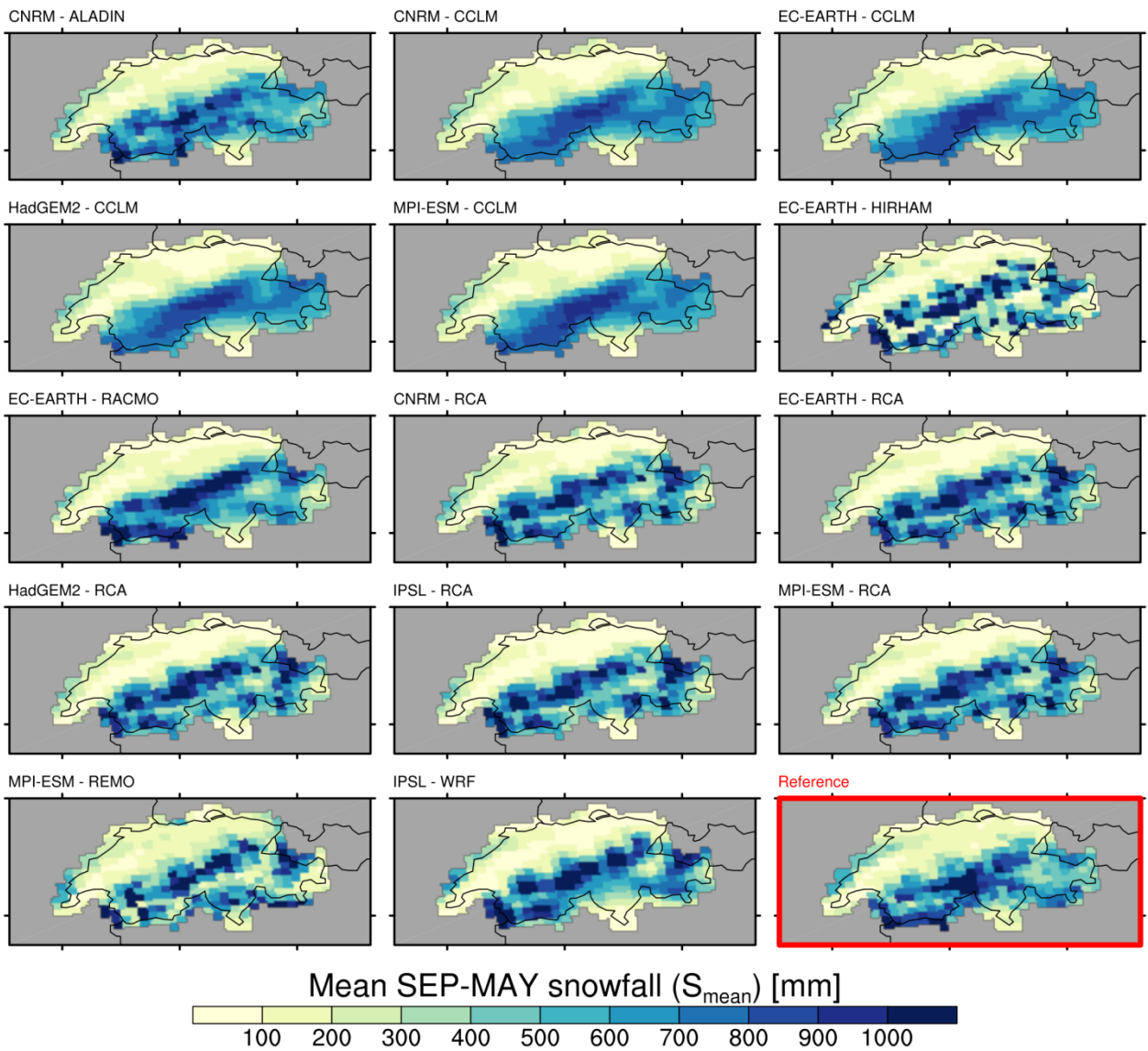
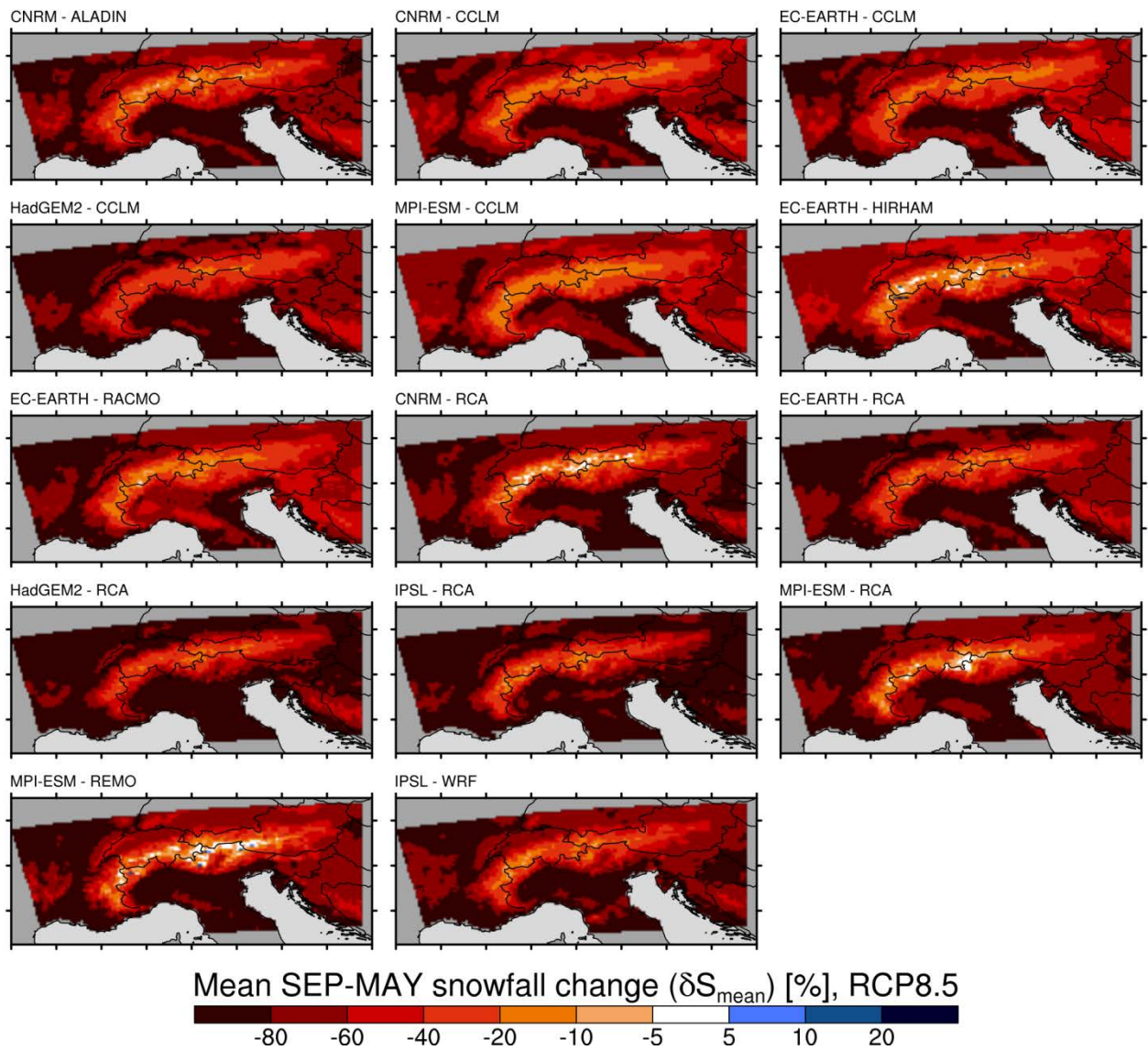


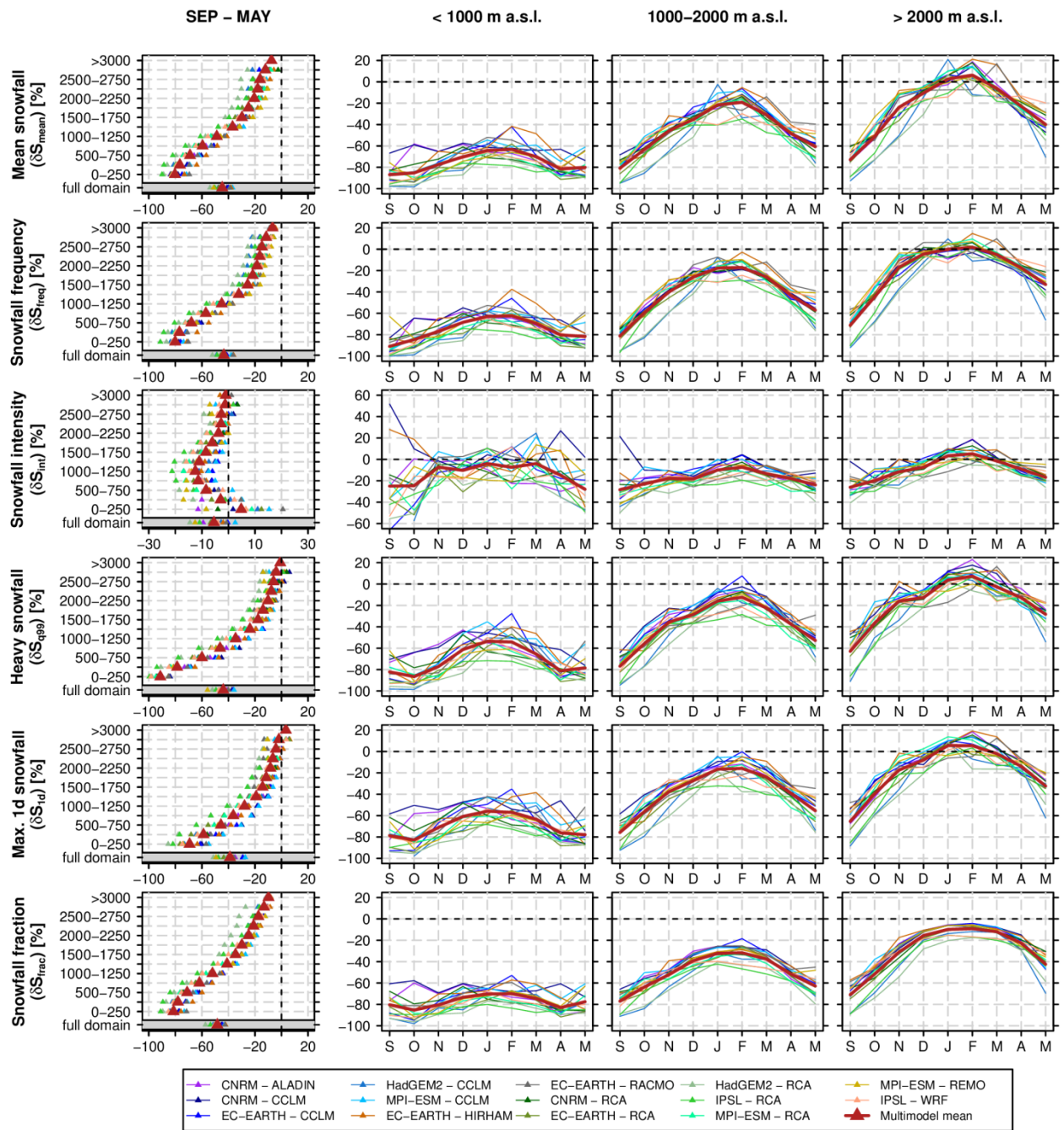
Figure 6 Spatial distribution of mean September-May snowfall, S_{mean} , in the EVAL period 1971-2005 and for the 14 snowfall separated + bias-adjusted RCM simulations ($\text{RCM}_{\text{sep+ba}}$). In the lower right panel, the map of the observation-based reference is shown.



1046
1047

1048 **Figure 7** Spatial distribution of relative changes (SCEN period 2070-2099 with respect to CTRL period 1981-
1049 2010) in mean September-May snowfall, δS_{mean} , for RCP8.5 and for the 14 snowfall separated + bias-adjusted
1050 RCM simulations ($\text{RCM}_{\text{sep+ba}}$). For RCP4.5, see Fig. S6.

1051

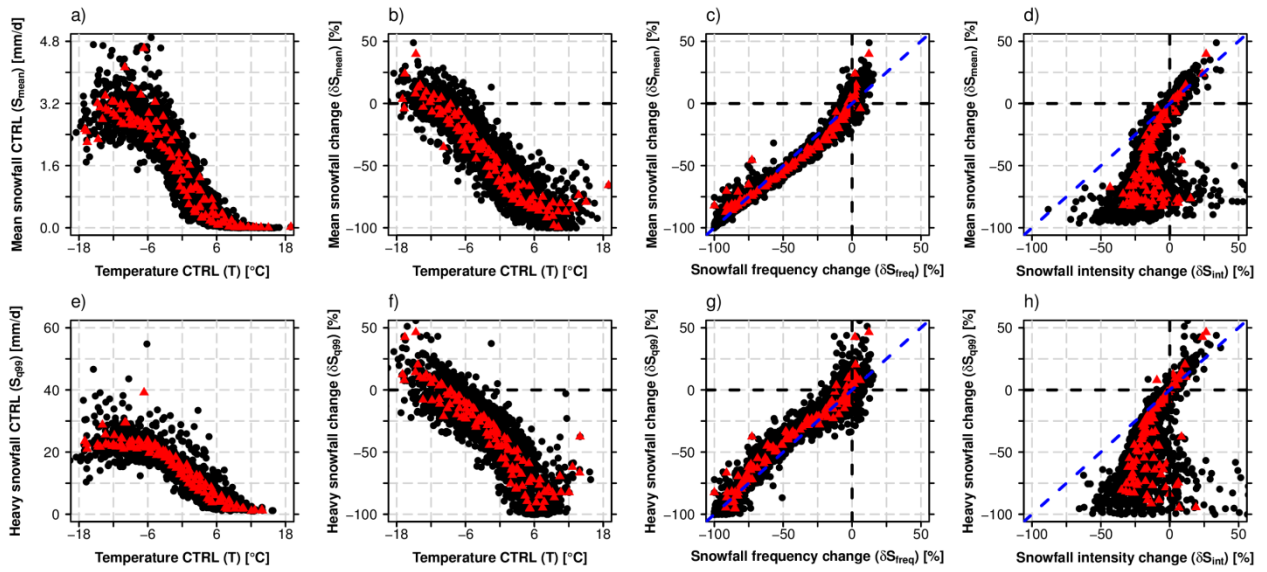


1052

1053

1054 **Figure 8** Relative changes (SCEN period 2070-2099 with respect to CTRL period 1981-2010) of snowfall indices
 1055 based on the 14 snowfall separated + bias-adjusted RCM simulations ($\text{RCM}_{\text{sep+ba}}$) for RCP8.5. The first column
 1056 shows the mean September-May snowfall index statistics vs. elevation while monthly snowfall index changes
 1057 (spatially averaged over the elevation intervals < 1000 m a.s.l., 1000 m a.s.l.- 2000 m a.s.l. and > 2000 m a.s.l.) are
 1058 displayed in columns 2-4.

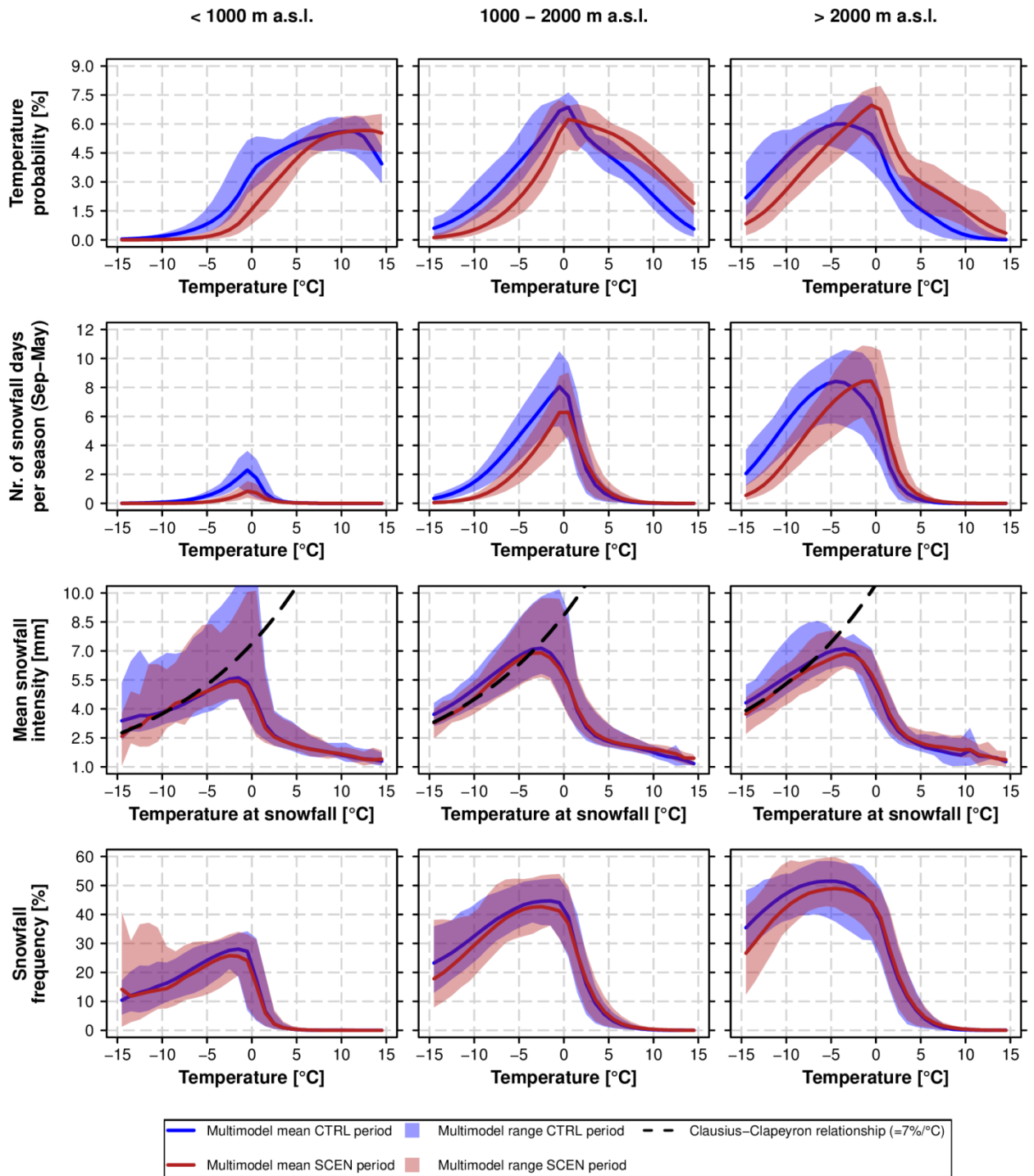
1059



1060
1061

1062 **Figure 9** Intercomparison of various snowfall indices and relationship with monthly mean temperature in CTRL.
 1063 For each panel, the monthly mean statistics for each 250 m elevation interval and for each of the 14 individual
 1064 GCM-RCM chains were derived (black circles). Red triangles denote the multi-model mean for a specific month
 1065 and elevation interval. The monthly statistics were calculated by considering all grid points of the specific
 1066 elevation intervals which are available for both variables in the corresponding scatterplot only (area consistency).
 1067 The data were taken from the 14 snowfall separated + bias-adjusted (RCM_{sep+ba}) RCM simulations. Relative
 1068 changes are based on the RCP8.5 driven simulations (SCEN 2070-2099 wrt. CTRL 1981-2010).

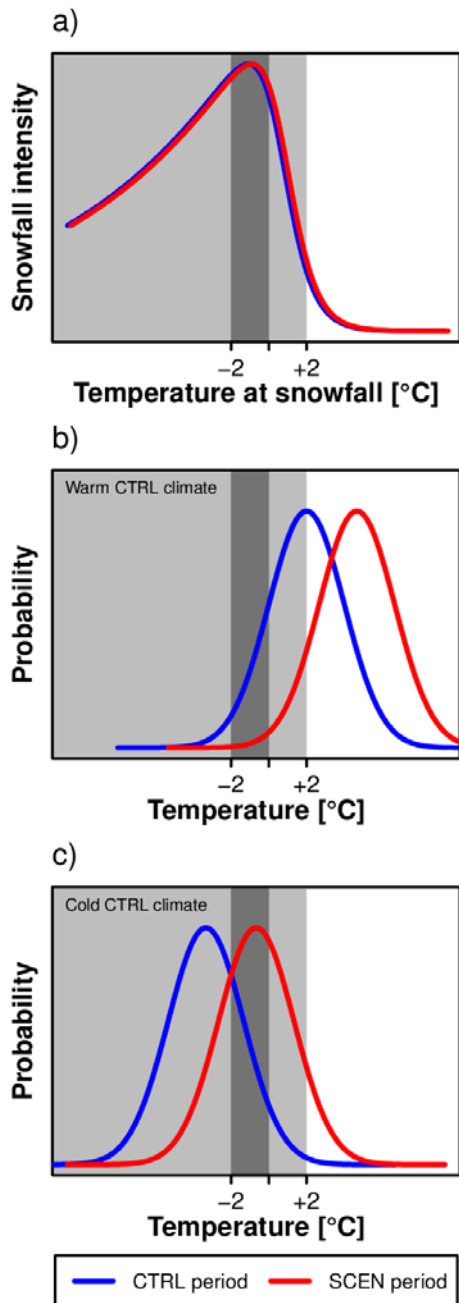
1069



1070

1071

1072 **Figure 10** Comparison of temperature probability, snowfall probability and mean snowfall intensity for the CTRL
1073 period 1981-2010 and SCEN period 2070-2099 for RCP8.5. The analysis is based on data from the 14 snowfall
1074 separated + bias-adjusted RCM simulations (RCM_{sep+ba}). The top row depicts the PDF of the daily temperature
1075 distribution, while the second row shows the mean number of snowfall days between September and May, i.e.,
1076 days with $S > 1$ mm (see Tab. 2), in a particular temperature interval. The third row represents the mean snowfall
1077 intensity, S_{int} , for a given snowfall temperature interval. In addition the Clausius-Clapeyron relationship, centred at
1078 the -10°C mean S_{int} for SCEN, is displayed by the black dashed line. PDFs and mean S_{int} were calculated by
1079 creating daily mean temperature bins of width 1°C .

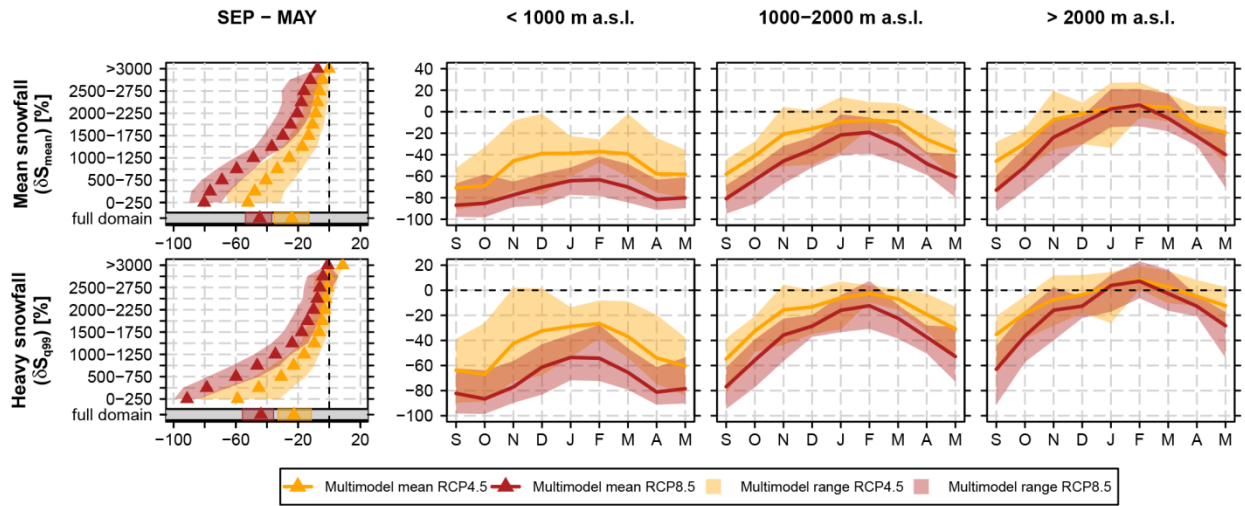


1080

1081

1082 **Figure 11** Schematic illustration of the control of changes in snowfall intensity on changes in mean and extreme
 1083 snowfall. a) Relation between temperature and mean snowfall intensity. b) Daily temperature PDF for a warm
 1084 control climate (low elevations or transition seasons, i.e., beginning or end of winter). c) Daily temperature PDF
 1085 for a cold control climate (high elevations or mid-winter). The blue line denotes the historical CTRL period, the red
 1086 line the future SCEN period. The light grey shaded area represents the overall temperature interval at which
 1087 snowfall occurs, the dark grey shading shows the preferred temperature interval for heavy snowfall to occur.

1088



1089

1090

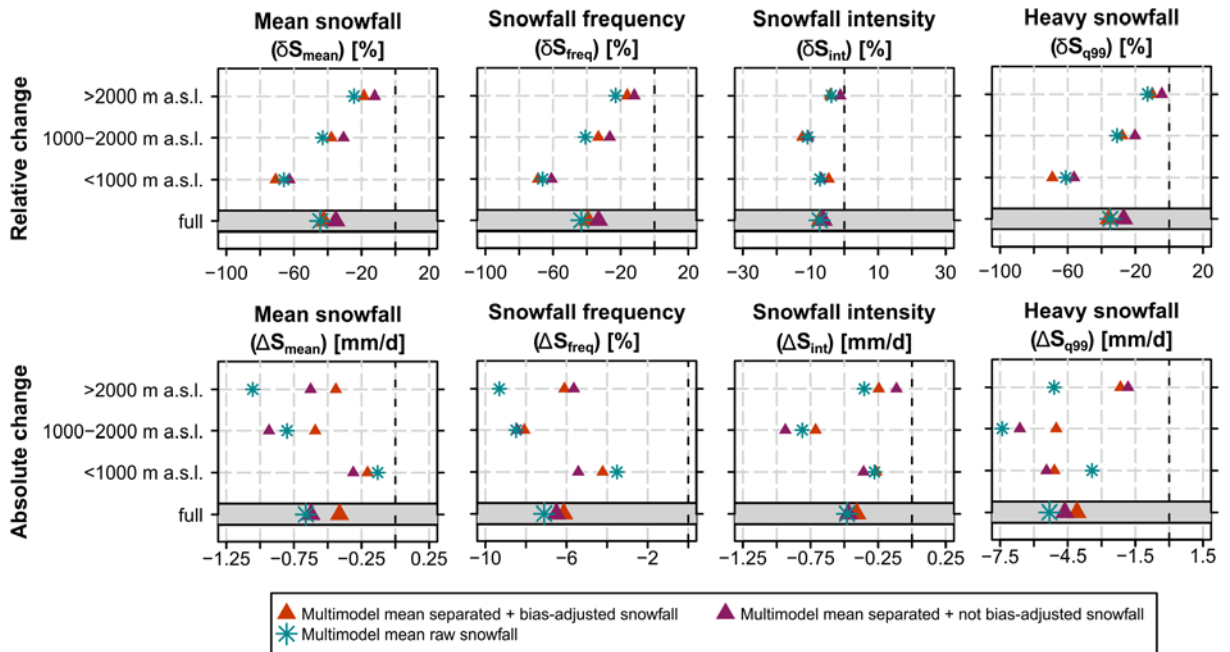
1091

1092

Figure 12 Similar as Figure 8 but showing projected changes of mean snowfall, δS_{mean} , and heavy snowfall, δS_{q99} , for the emission scenarios RCP4.5 and 8.5. See Fig. S9 for the emission scenario uncertainty of the remaining four snowfall indices.

1093

1094
1095



1096
1097
1098
1099
1100

Figure 13 Relative and absolute changes (SCEN period 2070-2099 with respect to CTRL period 1981-2010) of mean September-May snowfall indices based on a subset of 9 snowfall separated + bias-adjusted ($\text{RCM}_{\text{sep+ba}}$), 9 snowfall separated + not bias-adjusted ($\text{RCM}_{\text{sep+nba}}$) and 9 raw snowfall RCM simulations (RCM_{raw}) for RCP8.5. Only RCM simulations providing raw snowfall as output variable (see Tab. 1) were used in this analysis.

1101

1102 **Tables**

1103

1104 **Table 1** Overview on the 14 EURO-CORDEX simulations available for this study. The whole model set consists of
 1105 seven RCMs driven by five different GCMs. All experiments were realized on a grid, covering the European
 1106 domain, with a horizontal resolution of approximately 12 km (EUR-11) and were run for control RCP4.5 and
 1107 RCP8.5 scenarios within the considered time periods of interest. A subset of 9 simulations provides raw snowfall,
 1108 i.e., snowfall flux in kg/m²s, as output variable. For full institutional names the reader is referred to the official
 1109 EURO-CORDEX website www.euro-cordex.net. Note that the EC-EARTH-driven experiments partly employ
 1110 different realizations of the GCM run, i.e., explicitly sample the influence of internal climate variability in addition to
 1111 model uncertainty.

RCM	GCM	Acronym	Institute ID	Raw snowfall output
ALADIN53	CNRM-CERFACS-CNRM-CM5	CNRM - ALADIN	CNRM	no
CCLM4-8-17	CNRM-CERFACS-CNRM-CM5	CNRM - CCLM	CLMcom/BTU	no
CCLM4-8-17	ICHEC-EC-EARTH	EC-EARTH - CCLM	CLMcom/BTU	no
CCLM4-8-17	MOHC-HadGEM2-ES	HadGEM2 - CCLM	CLMcom/ETH	no
CCLM4-8-17	MPI-M-MPI-ESM-LR	MPI-ESM - CCLM	CLMcom/BTU	no
HIRHAM5	ICHEC-EC-EARTH	EC-EARTH - HIRHAM	DMI	yes
RACMO22E	ICHEC-EC-EARTH	EC-EARTH - RACMO	KNMI	yes
RCA4	CNRM-CERFACS-CNRM-CM5	CNRM - RCA	SMHI	yes
RCA4	ICHEC-EC-EARTH	EC-EARTH - RCA	SMHI	yes
RCA4	MOHC-HadGEM2-ES	HadGEM2 - RCA	SMHI	yes
RCA4	IPSL-IPSL-CM5A-MR	IPSL - RCA	SMHI	yes
RCA4	MPI-M-MPI-ESM-LR	MPI-ESM – RCA	SMHI	yes
REMO2009	MPI-M-MPI-ESM-LR	MPI-ESM – REMO*	MPI-CSC	yes
WRF331F	IPSL-IPSL-CM5A-MR	IPSL - WRF	IPSL-INERIS	yes

* r1i1p1 realisation

1112

1113

1114 **Table 2** Analysed snowfall indices. The last column indicates the threshold value in the CTRL period for
 1115 considering a grid cell in the climate changes analysis (grid cells with smaller values are skipped for the
 1116 respective analysis); first number: threshold for monthly analyses, second number: threshold for seasonal
 1117 analysis.

Index name	Acronym	Unit	Definition	Threshold for monthly / seasonal analysis
Mean snowfall	S_{mean}	mm	(Spatio-)temporal mean snowfall in mm snow water equivalent (only "mm" thereafter).	1 mm / 10 mm
Heavy snowfall	S_{q99}	mm/d	Grid point-based 99% all day snowfall percentile.	1 mm / 1 mm
Max. 1 day snowfall	S_{1d}	mm/d	Mean of each season's or month's maximum 1 day snowfall.	1 mm / 1 mm
Snowfall frequency	S_{freq}	%	Percentage of days with snowfall $S > 1$ mm/d within a specific time period.	1 % / 1 %
Snowfall intensity	S_{int}	mm/d	Mean snowfall intensity at days with snowfall $S > 1$ mm/d within a specific time period.	S_{freq} threshold passed
Snowfall fraction	S_{frac}	%	Percentage of total snowfall, S_{tot} , on total precipitation, P_{tot} , within a specific time period.	1 % / 1 %

1118
 1119
 1120
 1121